JAERI-Review
97-007

PROGRESS REPORT ON SAFETY RESEARCH ON RADIOACTIVE WASTE MANAGEMENT FOR THE PERIOD April 1995 to March 1996

March 1997

(Eds.) Keiichi SEKINE, Susumu MURAOKA and Tsunetaka BANBA

日本原子力研究所
Japan Atomic Energy Research Institute

本レポートは，日本原子力研究所が不定期に公刊している研究報告書です。
入手の問合わせは，日本原子力研究所研究情報部研究情報課（〒319-11 茨城県那珂郡東海村）あて，お申し越しください。なお，このほかに財団法人原子力弘済会資料センター（〒319-11 茨城県那珂郡東海村日本原子力研究所内）で複写による実費頒布をおこなっております。

This report is issued irregularly.
Inquiries about availability of the reports should be addressed to Research Information Division, Department of Intellectual Resources, Japan Atomic Energy Research Institute, Tokai-mura, Naka-gun, Ibaraki-ken 319-11, Japan.

編集兼発行　日本原子力研究所
印　　刷　㈱原子力資料サービス

JAERI－Review　97－007

放射性廃棄物処理処分の安全性研究に関する平成７年度報告書

日本原子力研究所東海研究所環境安全研究部
（編）関根　敬一・村岡　　進・馬場　恒孝

（1997年２月24日受理）

人工バリア研究室，天然バリア研究室及び地質環境研究室において，平成７年度に実施した放射性廃棄物処理処分の安全性に関する研究成果をまとめた。

その内容は次の通りである。

1）廃棄物固化体及び人工バリア材の研究開発では，各種固化体の性能評価試験を継続した。

2）浅地中埋設に関する安全評価研究では，土壌中の核種移行試験を継続した。

3）地層処分の安全性評価研究では，核種の水中での化学的挙動，地層中での核種移行，地下水流動に関する研究，並びに，ナチュラルアナログ研究を継続した。

東海研究所：〒319－11　茨城県那珂郡東海村白方白根２－４

JAERI－Review 97－007

Progress Report on Safety Research on Radioactive Waste Management for the Period April 1995 to March 1996

(Eds.) Keiichi SEKINE, Susumu MURAOKA and Tsunetaka BANBA

Department of Environmental Safety Research
Tokai Research Establishment
Japan Atomic Energy Research Institute
Tokai-mura, Naka-gun, Ibaraki-ken

(Received February 24, 1997)

This report summarizes the research and development activities on radioactive waste management at the Engineered Barrier Materials Laboratory, Natural Barrier Laboratory and Environmental Geochemistry Laboratory of the Department of Environmental Safety Research during the fiscal year of 1995 (April 1, 1995 - March 31, 1996) .

The topics are as follows:

1) As for waste forms and engineered barrier material, performance assessment studies were carried out on various waste forms.

2) In the safety evaluation study for shallow land disposal, migration behavior of radionuclides in a soil layer was studied.

3) In the safety evaluation study for geological disposal, chemical behavior of radionuclides in water, nuclide migration in geosphere and groundwater flow system were studied. Migration of uranium series nuclides in uranium ore deposit was studied as a part of natural analog study.

Keywords: High-level Waste, Low-level Waste, Waste Form, Engineered Barrier, Natural Barrier, Geosphere, Migration, Fixation, Natural Analog

Contents

目　　次

Introduction

In order to achieve the safe disposal of radioactive wastes, it is necessary to promote the development of waste management and safety assessment methodology.

The Japan Atomic Energy Research Institute (JAERI) has been conducting safety assessment study and development of new technology to contribute to the establishment of national system for the radioactive waste management in Japan.

This report summarizes the status and results of studies performed in the fiscal year 1995 at Engineered Barrier Materials Laboratory, Natural Barrier Laboratory and Environmental Geochemistry Laboratory of the Department of Environmental Safety Research, JAERI.

The progress report series have been issued in the following numbers:
JAERI-M 82-145, 83-076, 84-133, 85-090, 86-131, 87-131, 88-201, 89-192, 91-019, 92-022, 93-037, 94-027 and JAERI-Review 96-005.

1. Research and Development of Waste Forms and Engineered Barrier Materials

1.1 Performance of Ceramic and Glass Waste Forms

1.1.1 Density of Zirconia- and Alumina-based Ceramic Waste Forms

K.Kuramoto

INTRODUCTION

For the management of high concentrated TRU nuclides arising from a group partitioning process of high-level liquid waste, it is very important to isolate them from the biosphere for a long time. In the previous works, the applicability of yttria-stabilized zirconia (YSZ), alumina-compounds and YSZ-alumina composite ceramic waste forms for immobilizing high concentrated TRU nuclides were examined using TRU simulants with emphases on phase stability and chemical durability[1-3]. It was confirmed that YSZ, alumina-compound and YSZ-alumina composite waste forms indicated good phase stability, and that YSZ was superior to the compound and the composite waste forms for chemical durability. In this report, relation between density and crystal grain of the YSZ and the compound ceramic waste forms were investigated.

EXPERIMENTAL

Cerium oxide and/or Nd_2O_3 and a matrix of YSZ (TZ-8Y; Toso Co.Ltd.) or reagent grade of α-alumina were mixed using an agate mortar. After pelletization (~ 20 mmϕ), obtained disks were calcined at 1400 - 1500 ℃ for 80 hrs in flowing air for YSZ or 3%H_2 + Ar for the compound waste forms. Density measurement were performed by the Archimedes' method. Crystal grain observation in terms of shape and size of crystal grains were carried out using SEM (S-650; Hitachi).

RESULTS AND DISCUSSIONS

For YSZ waste forms, a pellet sample with a relative density of 96.7% ([5.955 g/cm^3 apparent density]/[6.158 g/cm^3 theoretical density]) was formed by sintering at 1400 ℃ in air. In Nd-bearing samples density decreased with an increase in the content of Nd however density of Ce-bearing samples were not change significantly by the variation of Ce content.

The crystal grain of the YSZ waste form was polyhedral with an average diameter of 8.7×10^{-6} m. This is due to the isotropic and marked grain growth based on the cubic system of YSZ. This grain growth results in the high-density pellet. For alumina-based ceramic waste form, densities tended to decrease with an increase in the content of the magnetoplumbite phase ($CeAl_{11}O_{18}$). The crystal grain of the magnetoplumbite phase was polygonal platelike. This anisotropic grain growth is due to the hexagonal system of this phase, and leads to low-density pellets. To produce a high-density pellets, it seems important to suppress the formation of the magnetoplumbite phase. It is also assumed for the YSZ-alumina composite waste forms that suppression of formation of the magnetoplumbite phase is necessary. For the examination of phase stability, chemical durability, and density, the YSZ waste form is confirmed to be superior to the alumina-based and the YSZ-alumina composite waste forms.

FUTURE WORK

In the future, the phase stability, chemical durability, mechanical properties, density, etc., of the YSZ waste forms doped with ^{237}Np or ^{241}Am or both will be investigated at the Nuclear Fuel Cycle Safety Engineering Research Facility (NUCEF) and the Waste Safety Testing Facility (WASTEF). A furnace that changes the atmosphere by the use of various gases, a hot-press furnace, atmosphere control devices and an off-gas treatment device are available in glove boxes for production of radioactive samples.

REFERENCES

(1) Kuramoto,K., et al.: Preprint 1993 Annu. Mtg. on Rare Earths, Tokyo, 2A07.
(2) Yanagi, T., et al.: J.Nucl.Sci.Technol., **31**[10], 1092 (1994).
(3) Sekine, K., et al,: JAERI-Reveiw 96-005, 2 (1996).

1.1.2 Alpha-decay Damage of Cm-doped Zirconolite

H. Mitamura

INTRODUCTION

In the polyphase titanate ceramic waste form, Synroc,[1] a part of actinide nuclides would be also incorporated in the zirconolite phase. Single phase material is useful for getting information about contribution of this phase to property changes of the polyphase material due to a-decay damage effects. In the present study, a-decay damage effects on zirconolite doped with ^{244}Cm (half-life, 18.1 years) were examined through density measurement and MCC-1 leach testing in WASTEF. Since the curium leaching in pure water was not sensitive to accumulation of a-decay damage, an acidic solution was used in the present study to prevent adsorption of the curium on specimen surfaces.

EXPERIMENTAL

The curium-doped zirconolite that had the nominal composition of $Ca_{0.975}(Cm,Pu)_{0.025}ZrTi_{1.975}Al_{0.025}O_7$ was hot-pressed using a graphite die at 1200。C and 29 MPa for 2 hr in a stream of N_2 gas. Flat faces and peripheries of cylindrical samples (2 cm in diam. x ~1 cm high) were polished with 6-mm diamond paste and #600 grit abrasive paper, respectively. The density of a polished cylinder was periodically measured at 30。C using the water displacement method.

Half-disk specimens were cut from the other polished cylinders. Flat faces of each half-disk specimen were also polished with 6-mm diamond paste. These flat faces were subjected to X-ray diffractometry before and after leach testing. Half-disk specimens that had accumulated doses of 1.5×10^{17} and 7.2×10^{17} a decays$\cdot g^{-1}$ were MCC-1 leach tested in pH~2 solution (0.05M KCl + 0.013M HCl) at 90。C for two months over four 7-day and a 28-day leach periods. The leachate samples were analyzed by g-ray spectrometry and inductively coupled plasma atomic emission spectroscopy (ICP-AES) for ^{244}Cm and calcium, respectively.

RESULTS AND DISCUSSION

Density

Density change of Cm-doped zirconolite is shown in Fig. 1 together with that of Cm-doped perovskite. The density changes are described well by linear lines. At a dose of 1.1×10^{18} a decays$\cdot g^{-1}$, the fractional density decrease of the Cm-doped zirconolite was 1.4%. In Fig. 1, the slope of the fitted line for the Cm-doped zirconolite is slightly gentler than that for

the Cm-doped perovskite. This phenomenon is consistent with the fact that perovskite had the largest unit-cell volume expansion in all Synroc constituent minerals.

Leach Testing

Figure 2 compares changes in pH and the Cm leach rate from the Cm-doped zirconolite which accumulated doses of (1) 1.5×10^{17} and (2) 7.2×10^{17} a decays$\cdot g^{-1}$. More damaged specimens were likely to give higher Cm leach rate. The Cm leach rate from these specimens decreased quickly after the initial 7-day leach period and then continued to decrease with time, while the Cm leach rate from the less damaged specimens was almost constant. In both specimens, pH was still buffered.

Figure 3 shows increments in Ca and Cm leach rates due to accumulation of a-decay damage. Both increment ratios are largest at the initial leach period, and decrease gradually and converge to a similar value (~0.7) at the end of leaching runs. More damaged specimens may increased Ca and Cm leach rates at the initial leach period, but it is possible that unknown soluble phases may contribute the increments of the leach rates.

X-ray diffractometry

X-ray diffractometry revealed that the phase assemblage after leaching was basically similar to that before leaching except an unknown soluble phase disappeared (Fig. 4). This unknown phase may be rich in Ca because Ca leach rate was considerably higher than the Cm leach rate.

CONCLUSION

The main results of the present study are as follows:

(1) Change in density of Cm-doped zirconolite reached 1.4% at a dose of 1.1×10^{18} a decays$\cdot g^{-1}$.

(2) More damaged specimens were likely to give higher Cm and Ca leach rates.

(3)The phase assemblage after leaching was basically similar to that before leaching except an unknown soluble phase disappeared.

REFERENCES

(1) A. E. Ringwood, S. E. Kesson, K. D. Reeve, D. M. Levins, and E. J. Ramm, "Synroc ," pp. 233-334 in *Radioactive Waste Forms for the Future*, Edited by W. Lutze and R. C. Ewing, Elsevier Science Publisher, New York, 1988.

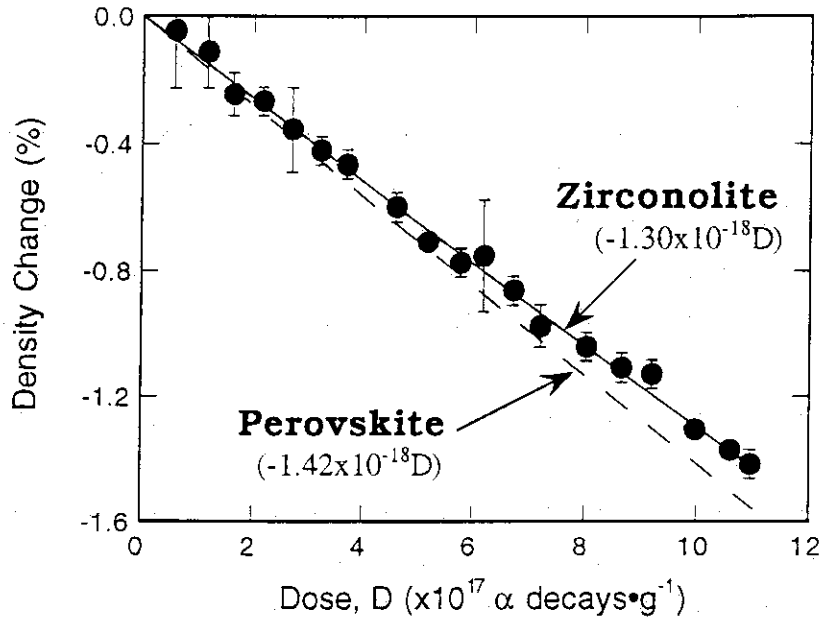

Fig. 1. Change in density of Cm-doped zirconolite versus α-decay dose.

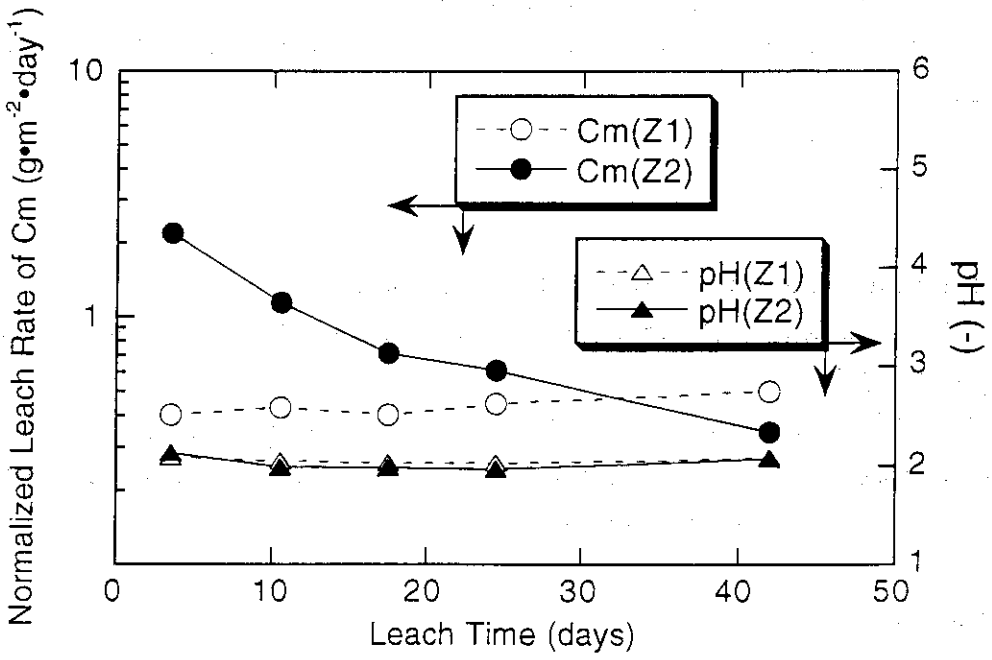

Fig. 2. Changes in normalized Cm leach rate and pH with time. The signs of Z1 and Z2 indicate the Cm-doped zirconolite specimens of doses of 1.5 x 10^{17} and 7.2 x 10^{17} α decays•g^{-1}, respectively.

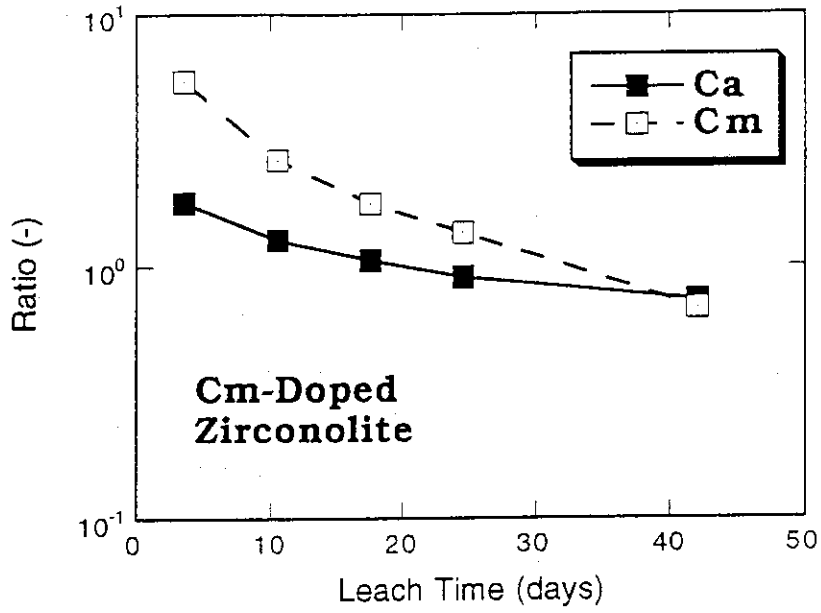

Fig. 3. Increment ratios for Ca and Cm leach rates between two doses: 1.5 x 10^{17} and 7.2 x 10^{17} α decays•g^{-1}. The ratio was obtained by dividing the leach rates at the latter dose by corresponding leach rates at the former dose.

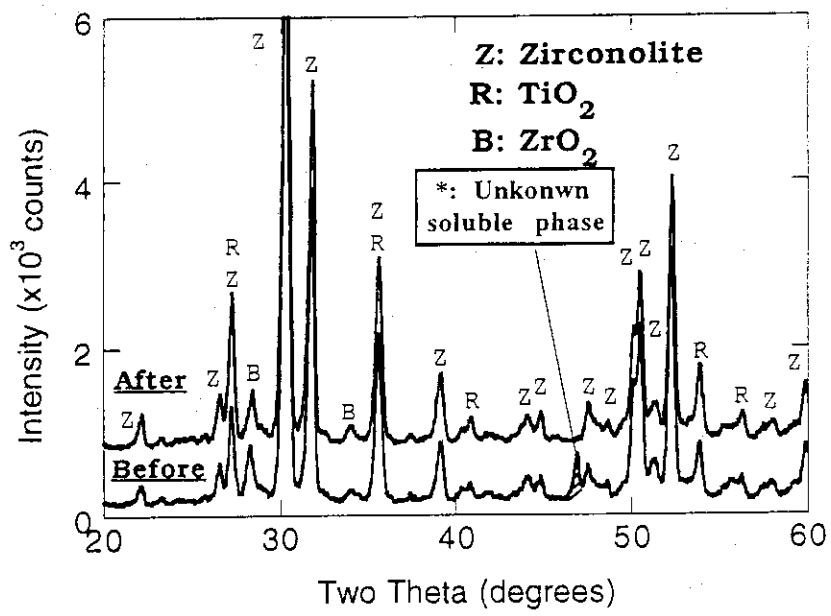

Fig. 4. X-ray diffraction patterns of Cm-doped zirconolite before and after leaching. Copper Kα radiation was used.

1.1.3 EFFECTS OF REDOX CONDITIONS OF WATER ON Pu AND Cm LEACHING FROM WASTE GLASS

T. Maeda

Introduction

In recent years, some corrosion tests on actinides-doped waste glasses have been performed, and leaching behavior of actinides from the waste glasses has been investigated. However, most of the previous corrosion tests have been performed under oxidizing conditions, and the leaching behavior of actinides under reducing conditions (predicted in repository environments) has not been well studied. Most of actinides contained in the waste glasses are redox active elements, and their oxidation states, chemical species and equilibrium solubilities are greatly influenced by redox conditions. Therefore, leaching behavior of actinides from the waste glasses can be greatly affected by redox conditions of water.

Experimental

The purpose of this study is to understand the effects of redox conditions of water on leaching behavior of actinides from the waste glasses. Static corrosion tests were carried out on the waste glass doped with Pu and Cm (PuO_2; 0.22wt%, Cm_2O_3; 0.09%) in deionized water at 90 ｡C with S/V ratio of 2500 m^{-1} under oxidizing and reducing conditions, respectively. The corrosion tests under oxidizing conditions were performed in air. While, the corrosion tests under reducing conditions were performed in the airtight stainless steel containers purged with mixed gas (Ar+5%H_2), where Eh of the solution was maintained at -0.45 V vs.SHE. After the corrosion tests, the solution was cooled to room temperature, and the solution pH and Eh were measured immediately. The solution was filtered through a 450nm filter and a membrane filter of NMWL 10,000 (1.8 nm in pore size) in order to investigate the distribution of the Pu and Cm particle size fractions. The solution concentrations of Pu, Cm and other glass constituent elements were measured by a-spectrometry and ICP-AES.

Results and Discussion

Fig. 1 shows the solution pH and Eh as a function of corrosion time, which shows that each redox condition was maintained sufficiently during the corrosion tests. Fig. 2 and Fig. 3 show the solution concentrations of Pu and Cm as a function of corrosion time under oxidizing and reducing conditions, respectively. It was observed that the redox conditions have no remarkable influence on the leaching behavior of Pu and Cm, which suggests that dominant oxidation states of the Pu and Cm in the solution under reducing conditions are the same as those under oxidizing conditions. It was also observed that the Pu and Cm concentrations in

the 1.8nm filtrate were one or two orders of magnitude lower than those in the 450nm filtrate under both oxidizing and reducing conditions. The Pu and Cm concentrations in the 1.8nm filtrate were assumed to correspond to the soluble species controlled by the solubility, and the difference in Pu and Cm concentrations between the 1.8nm and 450nm filtrates was assumed to correspond to the insoluble suspended fractions(colloidal particles). Therefore, it was suggested that the colloidal particles with the size from 1.8nm to 450nm are dominant phase for Pu and Cm in the solution under both oxidizing and reducing conditions. The experimental results also showed that the concentration of the colloidal particles of Pu and Cm was relatively high even in the early stage of glass corrosion, and almost saturated after 20days of corrosion time, which tendency is the same as other glass constituent elements such as Si, Ca and Al. While, the concentrations of the soluble species of Pu and Cm were very low in the early stage of glass corrosion, and they increased slowly with corrosion time. From these reslts, it is expected that formation of the colloidal particles of Pu and Cm are closely related to the leaching behavior of other glass constituent elements. Buck et al.[1] showed that clay colloids such as smectite and zeolite are produced as a direct result of the alteration of the waste glass itself, and they can sorb actinides. Therefore, the colloidal particles of Pu and Cm, which are dominant phase in the solution under both oxidizing and reducing conditions, are expected to be weakly crystalline clay colloids sorbing Pu and Cm (pseudocolloids) .

REFERENCE

[1] E.C.Buck, J.K.Bates et al., Mat.Res.Soc.Proc.Vol.294(1993)199.

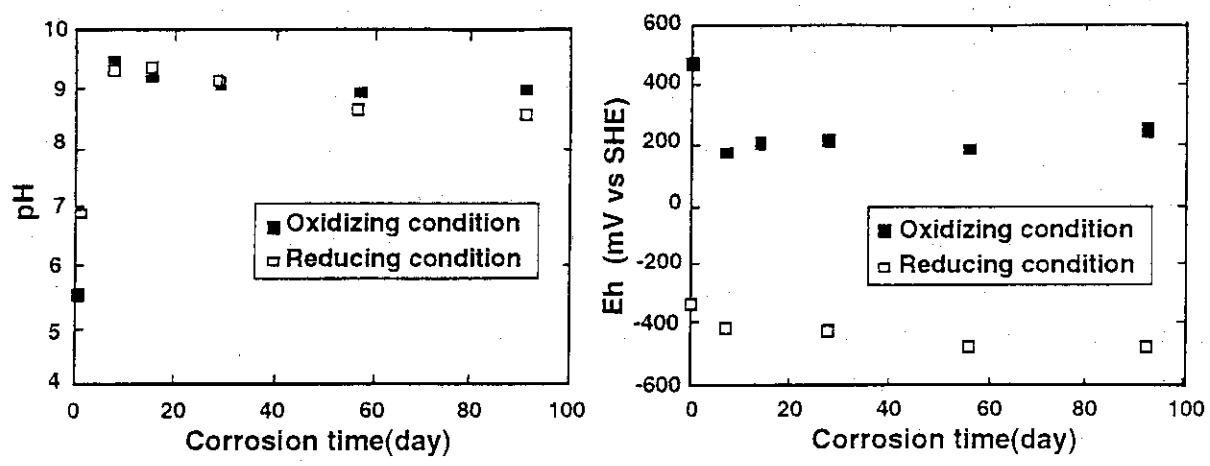

Fig.1. Solution pH and Eh as a function of corrosion time.

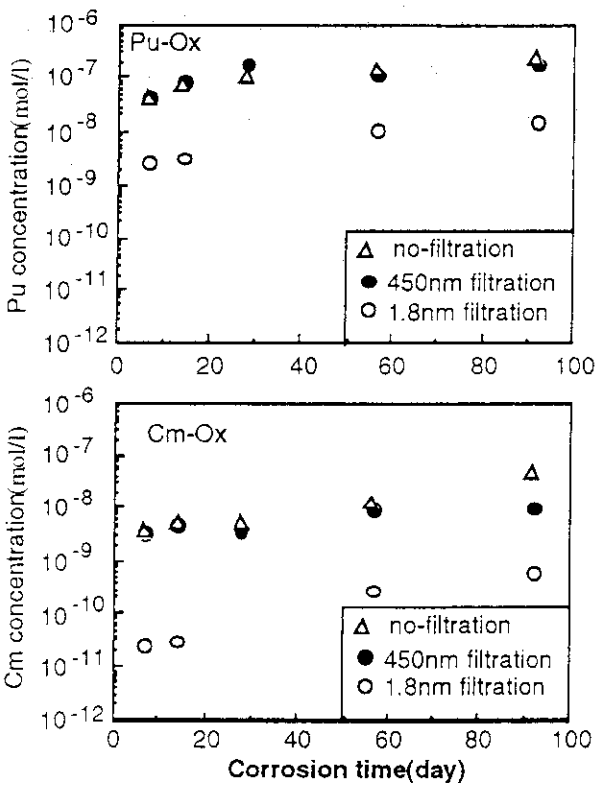

Fig.2. Solution concentrations of Pu and Cm as a function of corrosion time under oxidizing conditions.

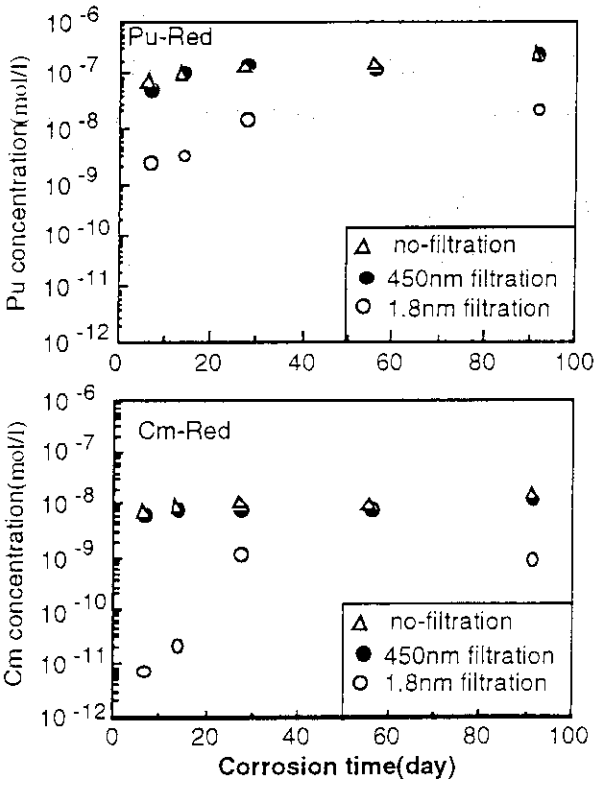

Fig.3. Solution concentrations of Pu and Cm as a function of corrosion time under reducing conditions.

2. Safety Evaluation Study on Shallow Land Disposal

2.1 Nuclide Migration Study

2.1.1 Colloidal Migration Behavior of Radionuclides Sorbed on Mobile Fine Soil Particles through a Sand Layer

T. Tanaka and T. Ohnuki

Introduction

Understanding the process of radionuclide migration in hydrogeologic environments is important in the assessment of radioactive waste disposal sites. Many radionuclides are readily sorbed on immobile geologic media and therefore are considered to be virtually immobile in the subsurface and to present little danger to groundwater supplies. McCarthy *et al.*, however, have described that colloids in the solid phase may be mobile in subsurface environments, so that, the colloids act as a third phase that can increase the amount of radionuclide flowing with groundwater[1]. In this study, migration experiments of ^{60}Co, ^{85}Sr and ^{137}Cs, which are critical hazards in low-level radioactive wastes, have been carried out by a column method using the pretreated sand layer in which fine soil particles can easily move with water flow, to obtain the information relating to migration of the pseudocolloidal radionuclides sorbed on mobile fine soil particles in soil layer. Sorption and desorption behaviors of the radionuclides on and from mobile fine soil particles, respectively, have been examined.

Experimental

Materials

The soil used in the present study was a coastal sandy soil, which was sampled at a site of the Tokai Research Establishment, Japan Atomic Energy Research Institute, Ibaraki, Japan. The coastal sandy soil was fractionated into two kinds of particle size ranges in diameter, by sieving method with JIS-standard sieve; one is fine soil of size range smaller than 37 μ m, and the other is coarse sand of size range from 250 to 350 μ m. The coarse sand was sufficiently washed with deionized water to remove fine soil particles, then the washed coarse sand was provided.

Radionuclides used were ^{60}Co, ^{85}Sr and ^{137}Cs in the form of chloride. A radioactive solution containing fine particles was prepared as follows: Two grams of the fine soil smaller than 37 μ m were mixed with 400 cm^3 of deionized water in a glass vessel. This mixed solution was filtrated with a membrane filter of 5 μ m in pore size, because some soil particles

larger than 7 μ m were trapped by a column layer of the coarse sand. And then the filtrate was spiked with the radionuclides to have concentrations of 10^2 Bq/cm^3 for ^{60}Co and ^{85}Sr and 10 Bq/cm^3 for ^{137}Cs. The spiked filtrate, called as a suspended radioactive solution in the present study, was used as an influent solution in column experiments.

Migration Experiments of Radionuclides Sorbed on Fine Particles

The experimental apparatus for examining the migration behavior of the radionuclides sorbed on the fine particles is schematically shown in **Fig. 1**. A column was made of glass and had the dimensions of 1.9 cm in diameter and 15 cm in height. A coarse sand column saturated with water was prepared by pouring the coarse sand into the column filled with deionized water, to be made a bed thickness of 1, 2, 4, 6, 8 or 10 cm. Bulk density and porosity of the coarse sand column were 1.6 g/cm^3 and 40 %, respectively. All the migration experiments were carried out at room temperature near 25 ℃.

The suspended radioactive solution of 10 cm^3 was introduced into each column by a micro tube pump at a constant flow rate of 2.8 cm^3/min (flow velocity in the coarse sand column: 2.5 cm/min). After inflowing the suspended radioactive solution, 40 cm^3 of deionized water were introduced into the column to flow out fine particles remaining in the column. Each effluent of 50 cm^3 in total volume was collected, and concentrations of radionuclides in the effluents were measured. It was comfirmed that all of the fine particles introduced into the coarse sand column are flowed out without any detainment by the coarse sand.

Results

Relationships between the lengths of the coarse sand column and the amounts of each radionuclide passed through the column are shown in **Fig. 2**, where a value at 0 cm in the column represents initial amount of each radionuclide sorbed on the fine particles in the suspended radioactive solution. In the reference tests, ^{85}Sr and ^{137}Cs were not detected in all effluents passed through the coarse sand columns between 1 and 10 cm in length, while ^{60}Co was detected to be 30 Bq. The detected ^{60}Co is attributable to cobalt hydroxides, $\{^{60}Co(OH)_2\}_n$[2]. The amounts of $\{^{60}Co(OH)_2\}_n$ were independent of the length of the columns. Hence the effluent amounts of ^{60}Co sorbed on the fine particles in Fig.2 were corrected by subtracting the amounts of $\{^{60}Co(OH)_2\}_n$, 30 Bq, from the total amounts of ^{60}Co in the effluents.

The effluent amounts of ^{85}Sr abruptly decreased within initial 1 cm in length of the coarse sand column, then gradually decreased with increasing length, followed by a constant value of 12 Bq at the length longer than 4 cm. The effluent amounts profiles of ^{60}Co and

^{137}Cs showed gradual decrease between 0 and 2 cm in length of the coarse sand column, followed by constant values of 9 Bq and 67 Bq, respectively, at the length longer than 4 cm. Thus, approximately 70 % of ^{60}Co and 90 % of ^{85}Sr sorbed on the fine particles were transferred to the coarse sand. Contrary to this, the amount of ^{137}Cs removed from the fine particles was little about 20 %.

Discussion

Above results show that some amounts of the radionuclides sorbed on the fine particles move to the coarse sand during the migration. And residual fractions of the radionuclides were irreversibly sorbed on the fine particles, because the fractions of radionuclides migrated through the coarse sand column of the length longer than 4 cm were constant. Thus, the radionuclides sorbed on the fine particles divided into two fractions; one is the fraction of the radionuclides sorbed reversibly on the fine particles, and the other is the fraction of the radionuclides fixed on the fine particles:

$$P_0=P_{rev0}+P_{fix} \quad (1)$$

where P_0 is initial amount of radionuclide sorbed on the fine particles (Bq), P_{rev0} initial amount of radionuclide sorbed reversibly on the fine particles (Bq), P_{fix} initial amount of radionuclide fixed on the fine particles (Bq). In the present experiments, P_{fix} is defined by the amounts of radionuclides migrated through the coarse sand column of the length longer than 4 cm.

Under the present experimental condition, the apparent desorption of the radionuclides from the fine particles to the coarse sand column can be described by the first order kinetic reaction:

$$\frac{\partial P_{revt}}{\partial t} = -kP_{revt} \quad (2)$$

where k is reaction rate constant for desorption process from the fine particles (1/min), Prevt amount of radionuclide sorbed reversibly on the fine particles after t minutes, and t the time (min).

Eq.(2) can be integrated, and P_{revt} is expressed by the following equation:

$$\ln P_{revt}=-kt+\ln P_{rev0}. \quad (3)$$

Since an amount of radionuclides remaining on the fine particles at t minutes after the introduction, P_t, is expressed by a sum of P_{revt} and P_{fix}, Eq.(3) can be changed into

$$\ln \frac{(P_t - P_{fix})}{(P_0 - P_{fix})} = -kt. \quad (4)$$

On the assumption that P_{fix} and $\{^{60}Co(OH)_2\}_n$ are kept at a constant throughout the migration experiments, the reaction rate constant k is obtained from the slope in plots of $\ln\{(P_t - P_{fix})/(P_0 - P_{fix})\}$ versus t.

The values of P_0, P_{fix}, P_{rev0} and $\{^{60}Co(OH)_2\}_n$ are regarded as constant each other in the present experimental condition, as summarized in **Table 1**. And t is fit for column length divided by flow velocity. The plots of $\ln\{(P_t - P_{fix})/(P_0 - P_{fix})\}$ versus t are shown in **Fig. 3**. The linear relations were found within 1 minute for ^{85}Sr, 2 minutes for ^{137}Cs and 3 minutes for ^{60}Co. The k for each radionuclide was determined by the linear regression on the plots, and is given in **Table 2**. The order of magnitude of the k is followed as $^{85}Sr > ^{137}Cs > ^{60}Co$.

The authors had found that approximately 20 % and 34 % of the ^{137}Cs sorbed on the sandy soil are the fraction extracted with a KCl solution and the residual fraction, respectively[3], and more than 50 % of ^{137}Cs sorbed on the sandy soil interact with layer silicates[4, 5]. Since clay mineral contents in the soil fraction of smaller size in diameter is higher than that of larger size, the fine particles contain much clay minerals rather than the coarse sand[6]. Thus, considerable amounts of ^{137}Cs were strongly and irreversibly sorbed on the fine particles. During the migration of the fine particles through the coarse sand columns, a fraction of ^{137}Cs sorbed on the fine particles can be desorbed into pore water, then be sorbed on the coarse sand by the same reaction as that described above. Since ^{137}Cs is not only strongly adsorbed onto the fine particles but also desorbed hardly from them, 80 % of ^{137}Cs sorbed on the fine particles can pass through the coarse sand columns, as shown in Fig.2.

It has been reported that most of the Sr^{2+} in a solution were reversibly sorbed on the chlorite and sericite[7]. In addition, approximately 99 % of ^{85}Sr sorbed on the sandy soil used could be desorbed by Ca^{2+}[3]. These show that ^{85}Sr sorbed on the fine particles and the coarse sand can be desorbed into the pore water. The volume of the coarse sand is quite larger than that of the fine particles, so that most of ^{85}Sr in pore water would be sorbed on the coarse sand. Thus, 90 % of ^{85}Sr sorbed on the fine particles are retained by the coarse sand during the migration through the columns. The characteristics that most ^{85}Sr is weakly and reversibly sorbed on the fine particles probably cause the abrupt decrease in effluent amounts of ^{85}Sr, as compared with ^{60}Co and ^{137}Cs in Fig.2.

The authors had found that the ^{60}Co sorbed on the sandy soil used in the present study is sequentially extracted by 43 % with a $CaCl_2$ solution, 11 % with a KCl solution and 43 % with a $NH_2OH \cdot HCl$ solution, respectively[3]. This indicates that approximately 40 % of the ^{60}Co are reversibly sorbed on the sandy soil, but more than 40 % of the ^{60}Co extracted with $NH_2OH \cdot HCl$ were associated with manganese oxides or oxyhydroxides[5, 8, 9]. These results prove that a portion of ^{60}Co is probably sorbed tightly on the fine particles. Therefore, ^{60}Co of approximately 30 % relative to the influent was detected in the effluents passed through the

coarse sand columns.

The reaction rate constants k of ^{60}Co and ^{137}Cs are small as compared with ^{85}Sr. However, the k of the three radionuclides is fast respect to the residual time of the fine particles in the coarse sand column. Therefore, the pseudocolloidal migration of radionuclides sorbed on the fine particles can not be controlled by the desorption kinetics but the association mechanisms in the interactions between the radionuclides and the fine particles, because all of the radionuclides sorbed reversibly on the fine particles are rapidly removed to the coarse sand.

Conclusion

The pseudocolloidal migration of radionuclides sorbed on the fine particles can not be controlled by the desorption kinetics, but the association mechanisms in the interactions between the radionuclides and the fine particles, because all of the radionuclides sorbed reversibly on the fine particles are rapidly removed to the coarse sand.

References

(1) McCARTHY,J.F., ZACHARA,J.M.: *Environ.Sci.Technol.*, **23**, 496 (1989).

(2) BASE,C.F., MESMER,R.E.: "*The Hydrolysis of Cations*", 238 (1976), John Wiley & Sons, New York.

(3) TANAKA,T.: *JAERI-Research 95-044*, (in Japanese), (1995).

(4) PARK,C.K., WOO,S.I., TANAKA,T., KAMIYAMA,H.: *J.Nucl.Sci.Technol.*, **29**[12], 1184 (1992).

(5) TANAKA,T., SRIYOTHA,K., KAMIYAMA,H.: "*Proceedings of the third international conference on nuclear fuel reprocessing and waste management (RECOD'91)*", 1011 (1991), Sendai, Japan.

(6) TANAKA,T., YAMAMOTO,T.: *J.At.Energy Soc.Jpn.*, (in Japanese), **30**[10], 933 (1988).

(7) OHNUKI,T.: *Radiochim.Acta*, 64, 237 (1994).

(8) CHAO,T.T.: *Soil Sci.Amer.Proc.*, **36**, 764 (1972).

(9) MEANS,J.L., CRERAR,D.A., BORCSIK,M.P.: *Geochim.Cosmochim.Acta*, **42**, 1763 (1978).

Table 1 Values of P_0, P_{fix}, P_{revo} and amount of $\{^{60}Co(OH)_2\}_n$

Radionuclide	P_0 (Bq)	P_{fix} (Bq)	P_{revo} (Bq)	$\{^{60}Co(OH)_2\}_n$ (Bq)
^{60}Co	33	9	24	30
^{85}Sr	103	12	91	－
^{137}Cs	85	67	18	－

Table 2 Rate constant, k, for each radionuclide desorbed from the fine particles to the coarse sand

Radionuclide	k (1/min)
^{60}Co	1.3
^{85}Sr	4.0
^{137}Cs	2.0

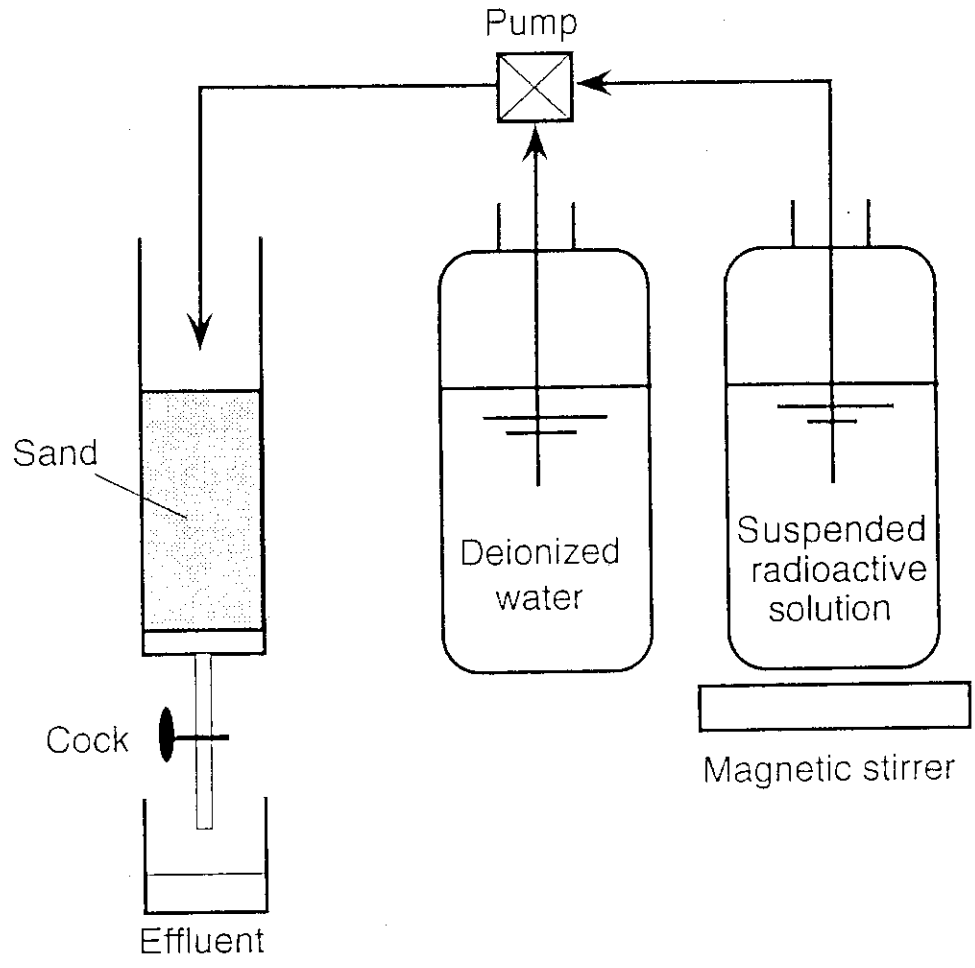

Fig.1 Schematic diagram of experimental apparatus for column method.

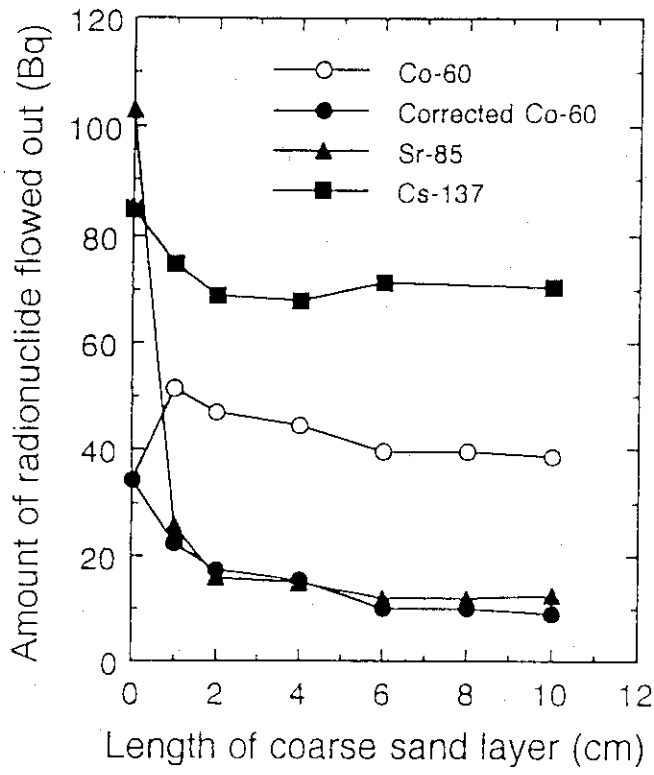

Fig.2 Relationships between length of coarse sand column and amount of radionuclide passed through the column; influent volume of the suspended radioactive solution 10 cm^3, flow rate 2.8 cm^3/min, flow velocity 2.5 cm/min. pH 6.7±0.3, temperature near 25℃, bulk density 1.6 g/cm^3. porosity 40 %. saturated water content.

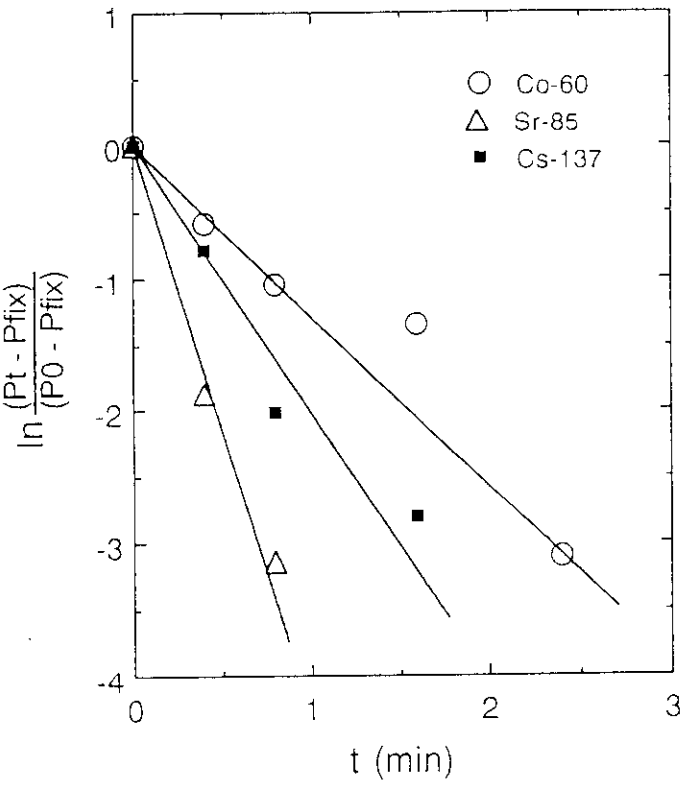

Fig.3 Plots of in{(P_t - P_{fix})/(P_0 - P_{fix})} versus t; P_t represents amounts of radionuclides remaining on the fine particles at t min, t is column length divided by flow velocity, P_0 and P_{fix} are listed in Table 1.

2.1.2 Sorption of Europium(III)-humate Complexes onto a Sandy Soil

S.Nagao, T.Tanaka and Y.Sakamoto

Introduction

Aquatic humic substances (humic and fulvic acids) are high-molecular-weight polymers and have a high complexation affinity for metal ions, especially trivalent and tetravalent actinides[1,2]. An enhancement of migration or retardation of actinides in underground layer is caused by the filtration and sorption properties of aquatic systems, depending on the molecular size distribution of humic substances[6]. In groundwaters, the bulk of actinide and lanthanide was associated with the humic colloids[3-5]. Aquatic humic substances are one of factors controlling the sorption behavior of actinides onto geologic materials. The purpose of this study was to investigate sorption behavior of actinides onto a sandy soil, which is a porous media in geologic environments, in the presence of humic acids (HAs). Europium(III) was used as a model substance of radioactive ^{241}Am and/or trivalent fission products. Effects of molecular size of HAs on the Eu (III) sorption were studied by high-performance gel permeation chromatography with ultraviolet and fluorescence detection.

Materials and methods

Materials

Four HAs from different origins were used in these experiments. A commercial HA was purchased from Aldrich Co. Ltd. (A-HA). A lake sedimentary HA was extracted from a lake sediment (H-HA) in Lake Haruna, Gunma prefecture, Japan. Two soil HAs were extracted from kuroboku soil at Ushiku (U-HA) and Mito (M-HA) in Ibaraki prefecture, Japan. All HAs were extracted and purified by the method of Hirata [7].

The characterization of HAs were carried out by spectroscopic and chromatographic methods. The UV-VIS spectra were measured with a Hitachi U-3310 UV-VIS spectrophotometer. The absorbance at 280 nm was 0.48 for A-HA, 0.17 for H-HA, 0.45 for U-HA and 0.38 for M-HA at the HA concentration of 20 mg/l, ionic strength of 0.1 M $NaNO_3$ and pH 7.0. The molecular size distribution of HAs were measured by high-performance gel permeation chromatography[8]. Chromatograms of the four HAs showed six peaks and their retention times were consistent among these samples (Fig. 1). The two distinct peaks were detected at shorter retention time of 9.0 minutes. The first distinct peak contained the molecular size fraction of more than 50,000 daltons. The peak height of the molecular size fraction increased in the order A-HA<H-HA <M-HA <U-HA. The peak height of second peak at retention time of 8.2-8.4 min increased in the order H-HA< M-HA< U-HA< A-HA. The peak height ratio (first/second peaks) was 0.71 for A-HA, 2.2 for H-HA, 2.4 for U-HA and 2.0 for

M-HA. These results indicate that the four HAs was divided into three groups: 1) Aldrich (A-HA); 2)Haruna (H-HA) and 3) Ushiku (U-HA) and Mito (M-HA).

Soil sample used in this study was from a coastal sandy soil at a site of the Tokai Research Establishment, Japan Atomic Energy Research Institute. The soil sample was air-dried and sieved into a size range from 250 to 300 μm, and then washed with deionized water. The main chemical composition was SiO_2 (78.2%) and Al_2O_3 (8.31%). The main minerals were quartz and feldspar.

Procedure

Sorption experiments of Eu(III) on the sandy soil were carried out by a batch method in the absence and presence of HAs. The 0.5 g sandy soil was mixed with 0.1 M $NaNO_3$ solution (9 ml) in a glass centrifuge tube with a screw cap. The solution with the soil was gently agitated on a reciprocal shaker for 7 days at 60 rpm. After the shaking, the pH was adjusted with dilute HNO_3. The 1 ml of HA stock solution with the concentration of 200 mg/l and 100 μl of Eu stock solutions (Eu concentration of 10^{-2} M, pH 5.5 and ionic strength of 0.1M) were added to the 0.1 M $NaNO_3$ solution with the soil sample. The solution was also agitated on the shaker for 7 days at 60 rpm. After the sorption experiment, the liquid phase was separated by centrifugation for 30 min at 3,000 rpm and filtration with 0.45 μm Millipore filters. Blank experiments for Eu and HA were also carried out with the same procedure. Preliminary kinetic experiments showed that equilibrium was achieved after 3 days. At the Eu-HA sorption experiments, brownish precipitates of Eu-humate complexes were not detected by the naked eye. Final pHs of the solutions after the experiments were pH 7.5 for the Eu-soil system, pH 7.6-7.7 for the HA-soil system and pH 7.2-7.5 for the Eu-HA-soil system.

Analyses

The concentration of Eu(III) was determined by inductively coupled plasma-emission spectrometry before and after the sorption experiments, and the percentage of the Eu(III) sorbed on the sandy soil was estimated. The concentrations of HAs before and after the sorption experiments were measured with UV spectrometry and high-performance gel permeation chromatography (GPC). The pH of each filtered solution was measured with a pH-meter.

The molecular size of HAs was measured with high-performance GPC according to the method of Nagao and Senoo[8]. The approximate upper exclusion limit of the GPC column was molecular size of 50,000 daltons. The HA samples, 100 μl water volume, were injected into the GPC column with a carrier flow-rate of 1 ml/min. Mobile phase was 0.01 M tris-HCl buffer solution including 0.01 M NaCl at pH 8.0. Absorbance was monitored at 280 nm by the UV-visible (VIS) detector. In order to study the properties of Eu(III)-humate complexes,

fluorescence chromatography was measured by the high-performance GPC with the fluorescence (GPC-FL) detector at an excitation wavelength of 320 nm and emission wavelength of 430 nm. The void volume (Vo) and total effective column volume (Vt) of the column were about 7.4 min and 22.9 min, respectively. The relative standard deviation of integrated peak area was less than 6% for these HAs before and after the sorption experiments.

Ultrafiltration technique was combined with the GPC method to study the molecular size distribution. The HAs were filtered with simple ultrafiltration filters, Millipore Ultrafree CL filters having the nominal molecular size of cut-off 5,000 and 10,000 daltons, and then injected into the GPC column. Absorbance was monitored at 280 nm by the UV-VIS detector. Percentages of HAs with each molecular size in the original HAs were calculated from the integrated peak area of the chromatograms.

In order to check the presence of humate complexes, the experiment on the complex formation between Eu(III) and Aldrich HA was carried out at pH 5.5. Below pH 6.0, Eu is mainly dissolved as a trivalent ionic form in the absence of HAs. The experimental procedure was similar with that of the sorption experiments without the sandy soil. The concentrations of Eu(III) and HA were 10^{-5} M and 20 mg/l, respectively. The presence of the Eu-humate complexes was confirmed by the fluorescence quenching of HAs complexed with Eu. The fluorescence emission spectra of the HA before and after the experiment were measured with a Hitachi F-4500 fluorescence spectrophotometer at excitation wavelength of 325 nm.

Results

Sorption of Eu on sandy soil

The amount of HAs sorbed on the sandy soil was negligible (Table 1). In the absence of HA, 95% of Eu(III) was sorbed on the sandy soil. The sorption of Eu decreased from 95% to about 20% in the presence of HAs. On the other hand, the HAs were sorbed on the sandy soil in the presence of Eu. The percentages of sorption were 68% for A-HA, 77% for H-HA, 89% for U-HA and 90% for M-HA. The degree of sorption was different for A-HA, H-HA and for soil HAs (U- and M-HA).

Chromatograms of humic acids after sorption experiments

(a) UV detection

Chromatograms of the four HAs after the sorption experiments of HA-soil system were similar with those of HAs before the experiments. The chromatograms of HAs after the sorption experiments of Eu-HA-soil system were different from those of HAs before the experiments (Figs. 1 and 2). The chromatograms showed two distinct peaks at 7.4 and 8.1 min before the experiments. However, the peaks of HAs at shorter retention time of 8.4 min were not detected after the experiments. The chromatograms after the experiments showed three peaks at retention times of 9.0, 9.4 and 10.0 minutes. The difference in chromatograms

indicated that larger molecular size fraction of HAs was not detected at the chromatograms after the experiments.

The chromatograms of HAs with molecular size of less than 5,000 and 10,000 daltons before the experiments showed three peaks at shorter retention time of 11.0 minutes (Fig. 2). The first peak was detected at 8.7 min for the HAs with molecular size of less than 10,000 daltons, but 9.0 min for the HAs with molecular size of less than 5,000 daltons and for the HAs after the experiments. The retention times of second and third peaks (9.4 and 10.0 min) agreed well between all the chromatograms in Fig. 2. These results show that the chromatograms of HAs after the sorption experiments are basically similar with the HA having molecular size of less than 5,000 daltons before the sorption experiments. The HAs with molecular size of more than 5,000 daltons were not detected in the solutions after the sorption experiments except for the Aldrich HA, including some part of the molecular size fraction ranging from 5,000 to 10,000 daltons. These results indicate that major part of the HAs with molecular size of more than 5,000 daltons was complexed with Eu(III) and sorbed on the sandy soil in the presence of Eu(III).

The peak heights of three retention times (9.0, 9.4 and 10.0 min) after the sorption experiments decreased by 20% for H-HA, 40% for U-HA and 49% for M-HA as compared to those of HAs with MW of less than 5,000 daltons before the experiments. The peak height of A-HA before and after the experiment was similar. The HAs were divided into three groups as follows: 1) A-HA; 2) H-HA and 3) U-and M-HA. The groups are similar with those of characteristics of HAs. The amount of HAs remaining in the solutions after the sorption experiments depends on the characteristics of HAs.

(b) Fluorescence detection

Chromatograms of HAs before and after the sorption experiments were shown in Fig. 3. The chromatograms showed four peaks for HAs after the experiments and with molecular size of less than 5,000 daltons before the experiments. The retention times agreed among these samples. The fluorescence intensities of HAs after the experiments, however, decreased up to 30-60% of the HAs with molecular size of less than 5,000 daltons. The peak height ratio (9.4/9.0 min) of the HAs after the experiments was also 13-46% lower than that of the HAs with molecular size of less than 5,000 daltons. The peak area of the HAs after the experiments corresponded to 30-60% of that of less than 5,000 daltons.

Discussion

Percentages of HA fractionated with each molecular size to original HA were calculated from the integrated peak area of the chromatograms in Fig. 2 and 3. The HAs with molecular size of less than 5,000 daltons, remaining in the solution after the sorption experiments at pH 7.5, were 50-140% at the UV detection and 27-62% at the fluorescence

(FL) detection (Table 2). The differences in the percentages between the UV and FL detection were about 17-24% for the soil HAs (U-HA and U-HA), 42% for the lake sedimentary HA (H-HA) and 75% for the A-HA.

Fluorescence spectroscopy is an alternative for the analysis of complexes between humic substances and several metal ions[9,10]. Humic substances exhibit fluorescence that is quenched upon binding to a paramagnetic ion[9-11]. Europium is a paramagnetic ion and hence, it may quench fluorescence efficiently.

In order to check the fluorescence quenching, the experiment on the complex formation between Eu(III) and Aldrich HA was carried out at pH 5.5. The fluorescence spectra of the Aldrich HA before and after the complexation experiment were shown in Fig. 4 together with those of HAs after the sorption experiment of Eu-HA-soil system at pH 7.5. The fluorescence quenching of HA was observed for the solutions in the presence of Eu (III) in both complexation and sorption experiments. The fluorescence intensities decreased by 35% at the complexation experiment (pH 5.5) and by 47% at the sorption experiment (pH 7.5). High loading of the HA after the complexation experiment is considered to be the complexation of HA with Eu(III) depending on the molecular size distribution of HA and the concentration of Eu. The molecular size distribution after the sorption experiment was different from that of the complexation experiment. The molecular szie-dependency of complexes of Aldrich HA with Am(III) was observed at laboratory experiment[12]. The quenching of humic substances correlated exponentially with the concentrations of paramagnetic ions[9-11]. The fluorescence maximum of the HA was shifted from emission wavelength of 455 nm to 445 nm at the sorption and complexation experiments (Fig. 4). The shift may be related to the complexation sites and mechanisms.

The quenching effect of Eu on the fluorescence intensities of the HAs was also observed in chromatograms detected by the GPC-FL detection in all the samples (Table 2 and Figure 3). This indicated that Eu(III) was complexed with HAs having molecular size of less than 5,000 daltons in the solutions after the sorption experiments at pH 7.5. The difference in the quenching effects by binding with Eu(III) suggests that the complexation capacity is different for each HA.

The complexation of Eu with HAs was dominant in neutral pH region. The sorption of Eu-HA complexes to the sandy soil (main minerals: quartz and feldspar) was lower than Eu(III) itself (Table 1). Ledin et al. have shown that at a pH range from 6 to 10, the sorption of Eu-fulvic acid complexes to quartz was about 60% lower than those of Eu(III)[13]. The Eu(III)- and Am(III)-humate complexes were the predominant species at pH 6-8 and ionic strength of 0.02-0.7 M[14]. Humic acids mainly control the dissolved form of Eu(III) and the sorption behavior of Eu(III) on the sandy soil

Conclusion

The sorption of Eu(III) by a sandy soil was studied by batch experiments at pH 7.5 in the presence of four humic acid (HAs) from different origins. Percentages of Eu sorbed onto the sandy soil were 95% in the absence of HA and 17-25% in the presence of HAs. The HA fraction with molecular size of less than 5,000 daltons was remaining in the solution after the Eu-HA sorption experiments. Studies on fluorescence quenching of HAs indicated that the HA fraction was complexed with Eu(III). The sorption of Eu onto the sandy soil was decreased by the formation of complexes with the HAs.

(This report reconstructed a proceeding paper (published to Radiochimica Acta (1996), Volume 74 and page 245-249) of Migration 95 held at Saint Maro in France).

References

(1) G. R. Choppin, B. Allard, In: *Handbook on the Physics and Chemistry of the Actinides* (A. J. Freeman and C. Keller, eds.), Elservier, 1985, pp. 407-429.

(2) J. I. Kim, In: *Handbook on the Physics and Chemistry of the Actinides*, (A. J. Freeman and C. Keller, eds.), Elservier, 1986, pp. 413-455.

(3) N. Miekeley, M. G. R. Vale, T. M. Tavares, W. Lei, In: *Scientific Basis for Nuclear Waste Management V* (W. Lutz, ed.), 1982, pp.725-733.

(4) J. P. Dearlove, G. Longwarth, M. Ivanovich, J. I. Kim, B. Delakovitz, P. Zeh, Radiochim. Acta **52/53**, 83 (1991).

(5) J. I. Kim, P. Zeh, B. Delakowitz, Radiochim. Acta **58/59**, 147 (1992).

(6) D. I. Kaplan, P. M. Bertsch, D. C. Adriano, K. A. Orlandini, Radiochim. Acta **66/67**, 181 (1994).

(7) S. Hirata, J. Oceanogr. Soc. Japan. **39**, 203 (1983).

(8) S. Nagao, M. Senoo, In: *Humic Substances and Organic Matter in Soil and Water Environments: Characterization, Transformations and Interactions* (C. E. Clapp, M. H. B. Hayes, N. Senesi and S. M. Griffith, eds.), IHSS, 1996, pp.71-79.

(9) R. A. Saar, J. H. Weber, Anal. Chem. **52**, 2095 (1980).

(10) D. K. Ryan, C. P. Thompson, J. H. Weber, Can. J. Chem. **61**, 1505 (1986).

(11) K. Ghosh, M. Schnitzer, Soil Sci. Soc. Am. J. **45**, 25 (1981).

(12) T. Tanaka, M. Senoo, In: *Scientific Basis for Nuclear Waste Management XVIII* (T. Murakami and R. C. Ewing, eds.), 1995, pp.1013-1020.

(13) A. Ledin, S. Karlsson, A. Duker, B. Allard, Radiochim. Acta **66/67**, 213 (1994).

(14) Y. Takahashi, Y. Minai, Y. Meguro, S. Toyoda, T. Tominaga, J. Radioanal. Nucl. Chem., Lett. **186**, 129 (1994).

Table 1 Percentages of Eu(III) and humic acid (HA) sorbed on the sandy soil at Eu-soil, HA-soil and Eu-HA-soil systems.

Sample	Eu-Soil	HA-Soil	Eu-HA-Soil	
	Sorbed Eu (%)	Sorbed HA (%)	Sorbed Eu (%)	Sorbed HA (%)
Aldrich HA (A-HA)	95	0	24	68
Haruna HA (H-HA)	95	0	17	77
Ushiku HA (U-HA)	95	4	25	89
Mito HA (M-HA)	95	0	23	90

The relative standard deviation of integrated peak area was less than 6% for these HAs.

Table 2 Percentages of peak area on humic acids (HAs) remaining in the solution at the Eu-HA sorption experiment as compared with that of molecular size of less than 5,000 daltons before the experiments.

Sample	Peak area (%)	
	GPC-UV[a]	GPC-FL[b]
Aldrich HA (A-HA)	137[c]	62
Haruna HA (H-HA)	97	55
Ushiku HA (U-HA)	67	50
Mito HA (M-HA)	51	27

a high-performance gel permeation chromatography with UV detection
b high-performance gel permeation chromatography with fluorescence detection
c The Aldrich HA has the molecular size ranging from 5,000 to 10,000 daltons after the sorption experiments as shown in Fig. 2, so that the percentage is over 100%.
The relative standard deviation of integrated peak area was less than 6% for these HAs.

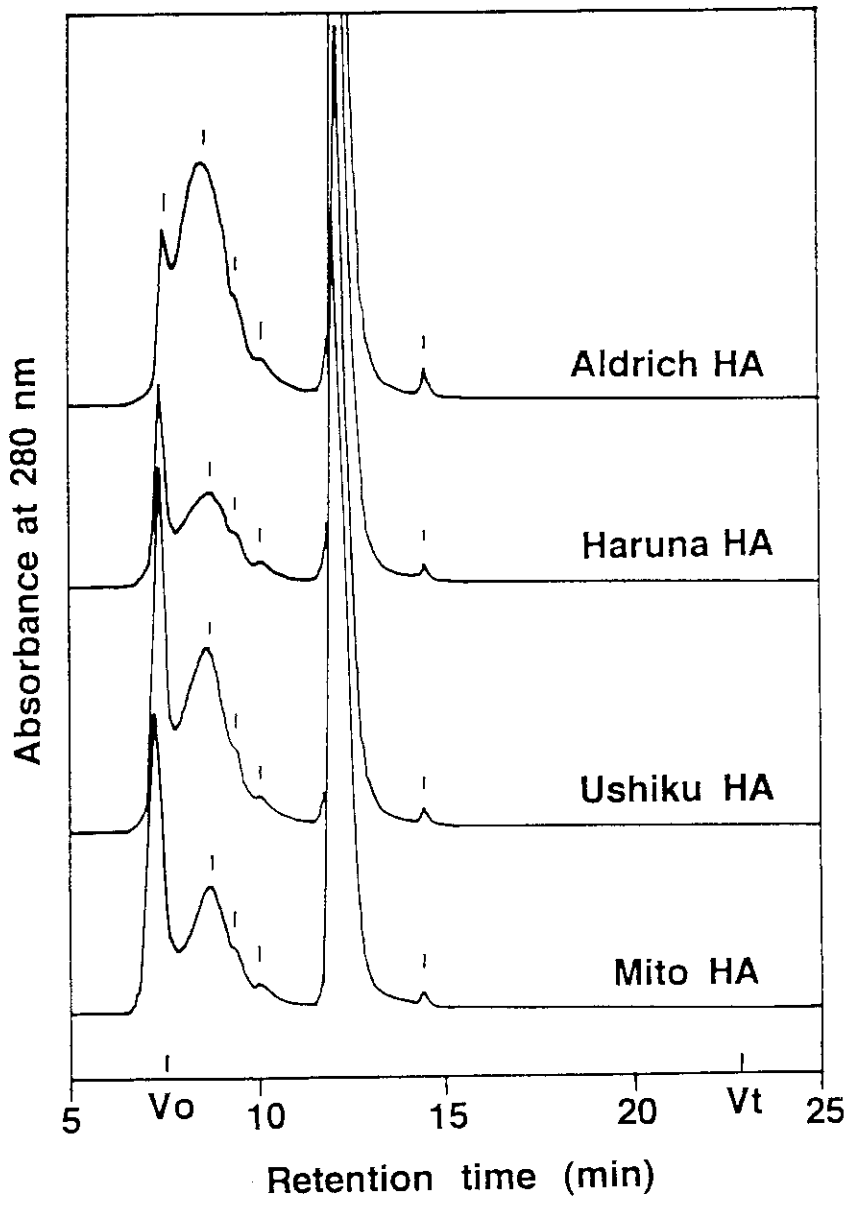

Figure 1. Chromatograms of humic acids from Aldrich Co. Ltd (A-HA), lake sediment (H-HA) and two kuroboku soil samples from Mito (M-HA) and Ushiku (U-HA). The chemical properties of sample solutions were as follows: HA concentration 20 mg/l; pH 7.5; ionic strength of 0.1 M $NaNO_3$. The fifth peak at 11.8 min was originated from $NaNO_3$.

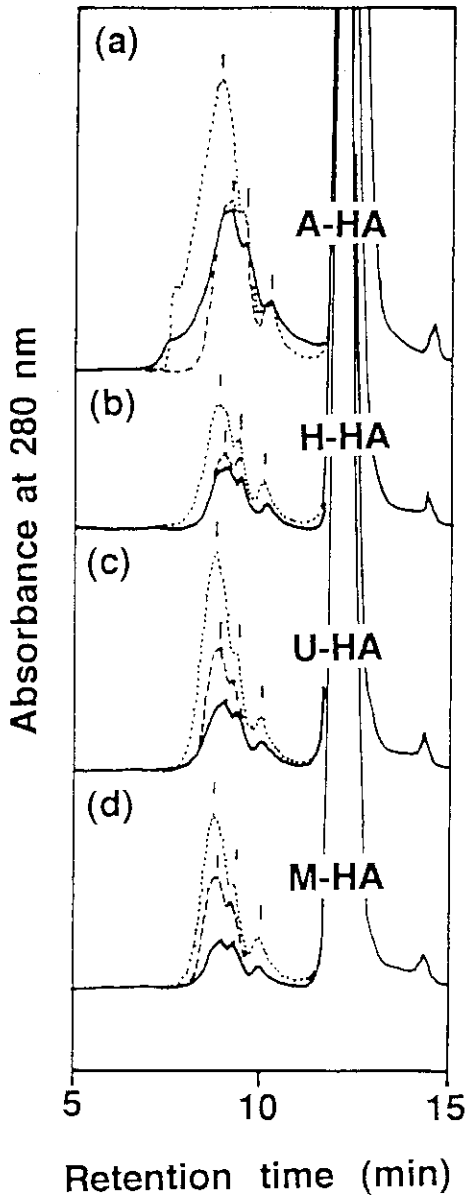

Figure 2. Chromatograms of humic acids from Aldrich Co. Ltd (a), Lake Haruna sediment (b) and two kuroboku soil samples from Ushiku (c) and Mito (d) after the sorption experiments of the Eu-HA-soil system. These data were measured with the high-performance GPC with a UV detector at UV 280 nm. The chromatograms of the solutions ultrafiltered by ultrafilters with the nominal molecular weight of cut-off 5,000 (dashed lines) and 10,000 daltons (dotted lines) before the sorption experiments are also shown. The absorbance unit in this figure is ten times greater than that in Fig. 1.

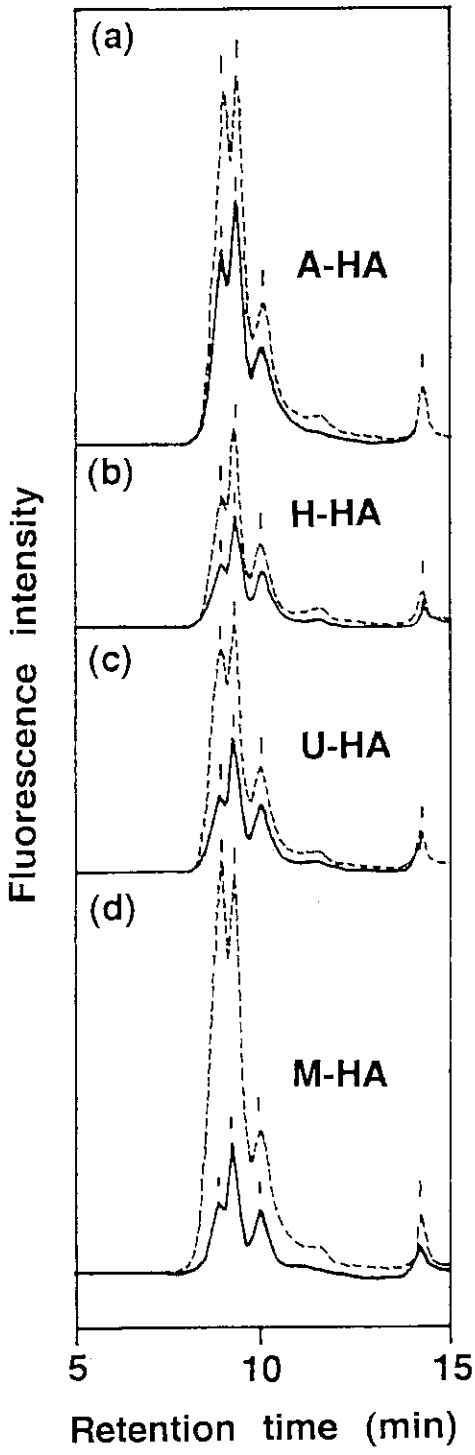

Figure 3. Chromatograms of humic acids from Aldrich Co. Ltd (a), Lake Haruna sediment (b) and two kuroboku soil samples from Ushiku (c) and Mito (d). These data were measured with the high-performance GPC with a FL detector at excitation 320 nm and emission 430 nm. The chromatograms of the solutions ultrafiltered by ultrafilters with the nominal molecular weight of cut-off 5,000 daltons (dashed lines) before the sorption experiments are also shown.

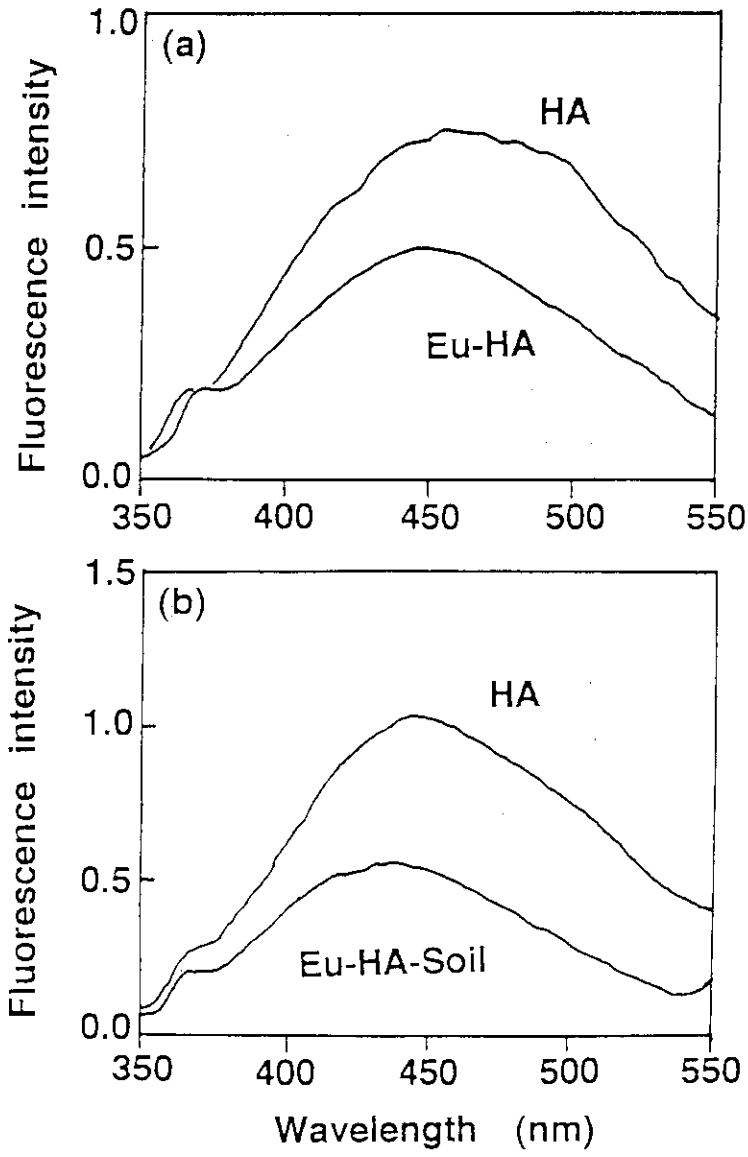

Figure 4. Fluorescence spectra of the Aldrich humic acid before and after the complexation experiments (a) and the humic acid before and after the sorption experiments of Eu-HA-soil system (b). The fluorescence emission spectra were measured at excitation wavelength of 325 nm. The pH was 5.5 for the complexation experiment and 7.5 for the sorption experiment.

3. Safety Evaluation Study on Geological Disposal

3.1 Chemical Behavior of Radionuclides in Water

3.1.1 Molecular Size Distribution of Np- and Am-fulvic Acid Complexes

S.Nagao, Y.Sakamoto, Y.Suzuki,* Y.Nakaguchi * and K.Hiraki*

Introduction

Molecular size is a convenient parameter for characterization of humic substances. The selective fractionation on the molecular size range of actinides and lanthanides occurred for the humic colloids in groundwater from the Gorleben[1,2] and for Aldrich humic acid in laboratory complexation experiments[3,4]. An enhancement of migration or retardation of actinides is caused by the filtration and sorption properties of aquatic systems, depending on the molecular size distribution of humic substances[5]. Molecular size of humic substances is a factor controlling the dissolved forms of actinides and their migration behavior in aquatic environments. This paper represents molecular size distribution of Np and Am in the presence of aquatic fulvic acid isolated from a river water.

Materials and method

Concentration and purification procedure

Aquatic fulvic acid (FA) was isolated from a river water collected at the Yamato River, which originates from the Kasachi mountain in Kinki area of Japan, followed by the XAD-8 method[6]. The 40L of the river water sample after the adjustment of pH 1.5 was flow into the column packed with Amberlite XAD-8 resin. The humic substances adsorbed on the resin were desorbed by NaOH solution. The alkali solution was acidified to pH 1.5 with HCl to precipitate humic acid (HA). The remaining solution containing FA was passed through the XAD-8 column. The FA was purified by immobilizing their acidified solution on XAD-8 resin. The FA was then extracted with 0.1M NaOH and passed through a column of hydrogen saturated AG MP-50 cation exchange resin to convert the FA to its hydrogen form. The purified HA and FA were freeze dried for chemical analysis and complexation experiment.

Characteristics of humic substances

The percentages of humic and fulvic acids were 12% and 88% of total humic substances, respectively. Fourier-transformed infrared (FT-IR) spectrum of the

FA was different from the HA at 1215 cm^{-1}, 1635 cm^{-1} and 1720 cm^{-1}, which correspond to the infrared adsorption band of aromatic C=C stretch and -C=O stretch of carboxyl group (Fig.1). The elemental composition of the FA was 48.08% C, 4.99% H, 2.87% N, 44.06% O on basis of FA normalized to 100wt% of organic components.

Complexation experiments

Complexation experiments for Np and Am were carried out in an ionic medium of 0.01M $NaClO_4$ and the concentrations of FA from 0, 2, 4, 7, 11, 14, 28, 50, 71 mg/l at pH 7.0. The concentrations of Np and Am were $6.8x10^{-6}$M and $7.6x10^{-9}$M, respectively. The solutions were shaken in an oven at 25 for 7 days. After the experiments, the pH was measured by a pH meter. These solutions were ultrafiltered with simple ultrafiltration filters, Millipore Ultrafree CL filters having nominal molecular weight of cut-off 100,000, 30,000, 10,000 and 5,000 daltons.

After the complexation experiments, brownish precipitates of FA complexes were not detected in the solutions for the Np complexation experiments, but formed for the Am complexation experiments at the FA concentration less than 7 mg/l. The percentages of Am precipitated were 76% in the absence of FA, 17% at 2 mg/l FA, 11% at 4 mg/l FA and 8% at 7 mg/l FA.

Analysis

The radioactive concentrations of ^{237}Np and ^{241}Am in each molecular size fractions were measured by a liquid scintillation counter. The amount of FA before and after the experiments was determined spectroscopically at ultraviolet wavelength of 280 nm. The corresponding concentration of FA was estimated from a calibration curve prepared from the same FA.

Results and discussion

Molecular size distribution of complexes

The molecular size distribution of Np, Am, FA and their complexes were shown in Fig.2. The FA consisted mainly of molecular size fraction less than 10,000 daltons (77 %). Np was dissolved as cationic forms with molecular size of less than 5,000 daltons on basis of calculation by MINTEQ. The percentage of Np-FA complexes with molecular size of 5,000 to 30,000 daltons was 7%.

The Am was dissolved as pseudocolloid with molecular size of more than 10,000 daltons in the absence of FA. The dominant molecular size was more than 100,000 daltons (66%). In the presence of FA, the major part of molecular size of

Am was shifted to the 10,000-100,000 daltons. The result indicates that Am was complexes with the FA.

Effects of FA concentration on complexation

The molecular size distribution of Am as a function of the FA concentration is shown in Fig.3. At the molecular size of more than 100,000 daltons, the percentages of Am was 66% in the absence of FA, 24% at 2-4 mg/l FA and 14?2% at 7-71 mg/l FA. The percentage of Am in 30,000-100,000 daltons increase with increasing the FA concentration of 0 to 7 mg/l and then constant (38 ?2%) above 7 mg/l FA. On the other hand, Am in molecular size of 10,000-30,000 daltons was 18% at 0 mg/l FA and 30?5% at 2-71mg/l FA. The percentages of Am in molecular size of 5,000-10,000 daltons and <5,000 daltons, not shown in Fig.3, were 15?3% and 4?1%, respectively. The molecular size distribution of Am, especially molecular size of 30,000-100,000 daltons and more than 100,000 daltons, was varied with the FA concentration from 0 to 4 mg/l and constant above 7 mg/l FA.

Conclusion

Molecular size distribution of Np and Am in the presence of fulvic acid, isolated from the river water, was studied by ultrafiltration. Am was selectively complexed with fulvic acid (FA) having molecular size of 10,000-100,000 (60%) at pH 7.0, ionic strength of 0.01M $NaClO_4$ and FA concentration of 2 to 71 mg/l. On the other hand, Np was dissolved as cationic form (90%) and the percentage of fulvate complexes was 7%. Characteristics of molecular size of FA are factors controlling the dissolved forms of actinide-fulvate complexes.

(This study was performed as a part of the Universities-Japan Atomic Energy Research Institute collaboration research project)

References

(1) Dearlove, J. P., Longwarth, G., Ivanovich, M., Kim, J.I., Delakovitz, B., Zeh, P.: Radiochim. Acta 52/53, 83 (1991).

(2) Kim, J. I., Zeh, P., Delakowitz, B.: Radiochim. Acta 58/59, 147 (1992).

(3) Tanaka, T., Senoo, M.: In: Scientific Basis for Nuclear Waste Management XVIII (T. Murakami and R. C. Ewing, eds.), 1995, pp.1013-1020.

(4) Sakamoto, Y., Nagao, S., Ohnuki, T., Senoo, M., Ohashi, A., Sato, S., Ohashi, H: In: Scientific Basis for Nuclear Waste Management XVIII (T. Murakami and R. C. Ewing, eds.), 1995, pp.997-1004.

(5) Kaplan, D. I., Bertsch, P. M., Adriano, D. C., Orlandini, K. A.: Radiochim. Acta 66/67, 181 (1994).

(6) Thurman, E. M. and Malcolm, R. L.: Environ. Sci. Technol., 15, 463 (1981).

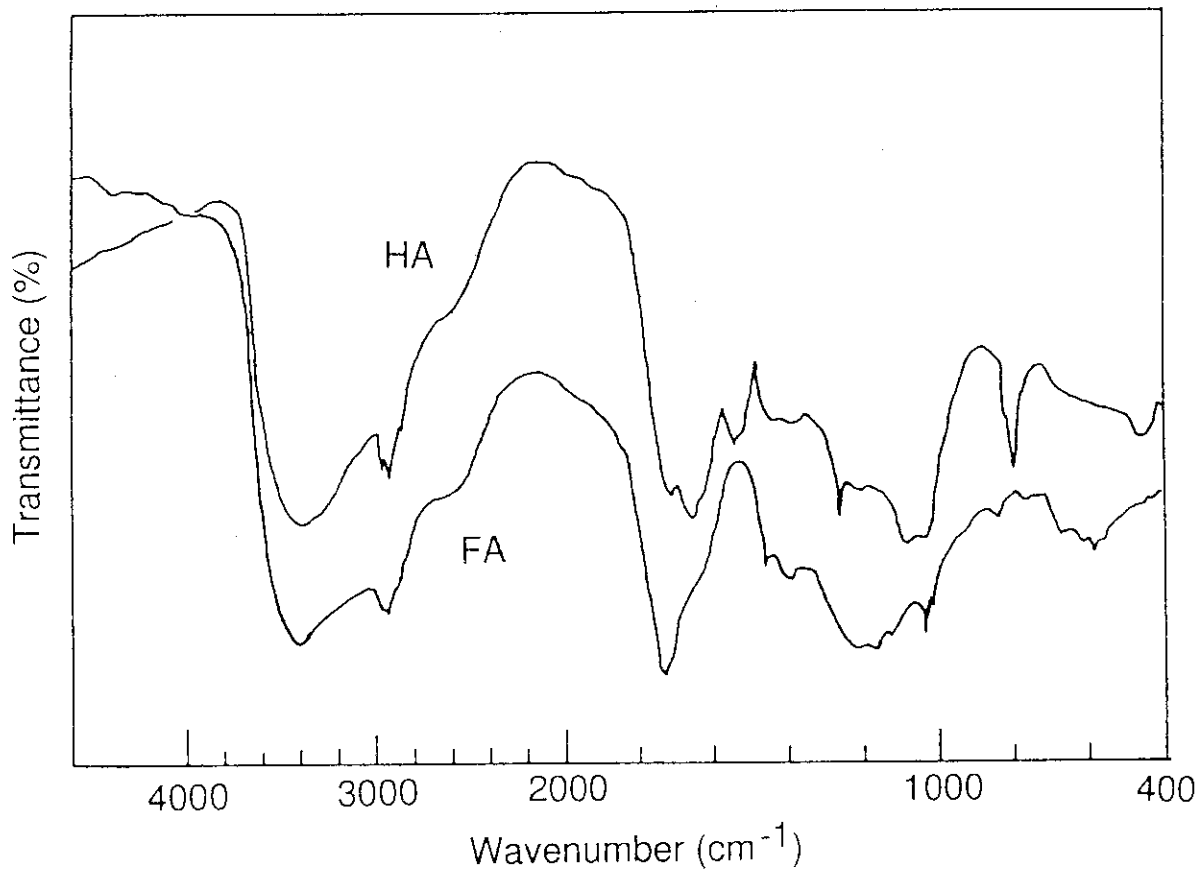

Fig.1 Fourier-transformed infrared (FT-IR) spectra of humic and fulvic acids isolated from the Kuji river water. The spectra were recorded on KBr disks with an FT-IR spectrophotometer.

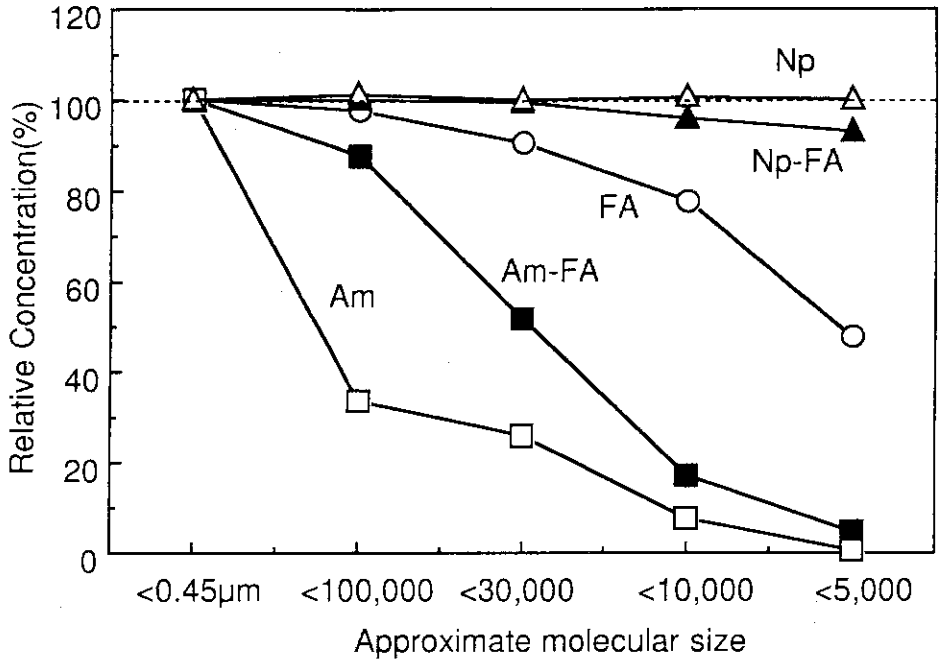

Fig. 2 Percentages of Np,Am, fulvic acid (FA) and their complexes in each molecular size fraction.

pH:7.2 I=0.01M FA:71mg/l Am:7.3×10^{-9}M Np:6.7×10^{-6} M

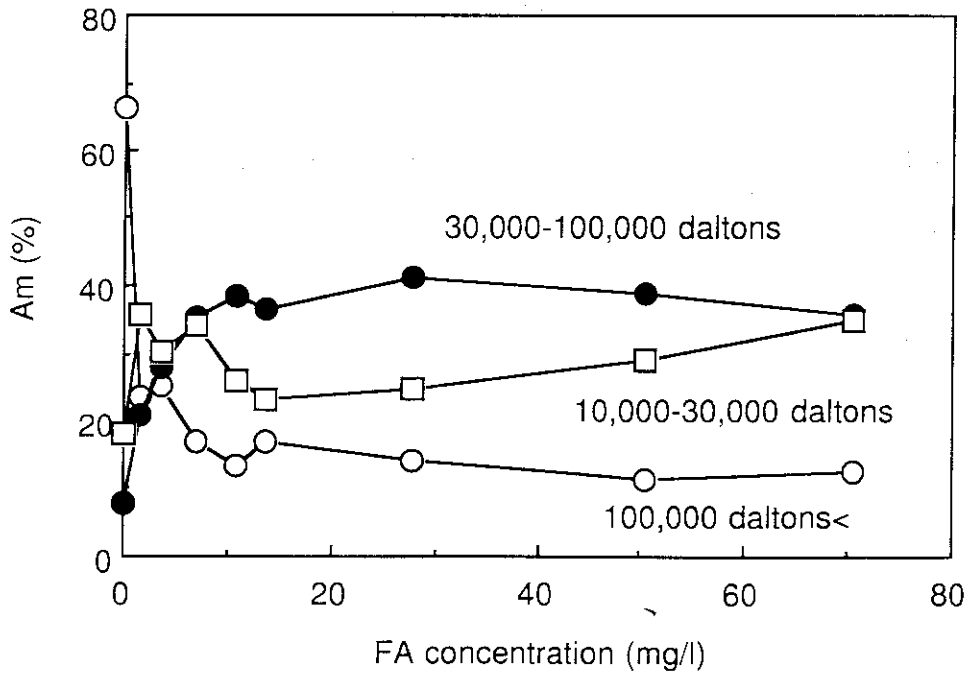

Fig. 3 Percentages of Am in molecular size of 10,000-30,000 daltons, 30,000-100,000 daltons and >100,000daltons as a functionof the fulvic acid concentration.

3.1.2 Effect of Complexation on Solubility of Neptunium(IV) in Aqueous Carbonate Solutions

S. NAKAYAMA and T. YAMAGUCHI

The solubility of neptunium(IV) hydrous oxide was studied in Na_2CO_3 and K_2CO_3 solutions from undersaturation direction at 25.0±0.2℃ in a controlled atmosphere containing high purity Ar (<1 ppm O2). Equilibration periods were up to 123 days.

The solubility was fairly low ($<10^{-8}$M) and constant in solutions with carbonate concentrations of <0.1M, and increased dramatically with the increase in the carbonate concentrations of >0.1M.

Solid characterization was made for the Np(IV) solid phases equilibrated with 0.01M, 0.2M Na_2CO_3, and 4.0M K_2CO_3 solutions for 67 days by X-ray diffractometry, UV-Vis-NIR and FT-IR photoacoustic spectroscopy. The results indicated that the solids formed in 0.01M and 0.2M Na_2CO_3 solutions were a poorly-crystalline hydrous oxide, and the solid in the 4.0M K_2CO_3 solution appeared to be non-crystalline and contained hydroxyl groups and carbonate ions.

This study is under way to investigate the solubility in bicarbonate solutions, which will helps us predict aqueous Np(IV) species.

3.1.3 Calculation of peak shifts of powder X-ray diffraction patterns caused by small crystals of goethite

Tetsushi NAGANO

Around repositories of high-level radioactive wastes, iron compounds generated as corrosion products of overpack material or as weathering products of iron-containing minerals are considered to be important in evaluation of radionuclide migration in geosphere because of their high fixation potential. In fact, the fixation of a small quantity of some elements by the iron compounds often occurs in the nature. The fixation mechanism has been successively-investigated in the laboratory by means of transmission electron microscopy (TEM), infrared spectroscopy (IR) and powder X-ray diffactometry (XRD), which enables us to qualitatively or quantitatively analyze crystalline phases, especially to determine lattice parameters. For determination of the lattice parameters, some accurate peak positions are required. Among iron minerals, goethite is one of the most wide-spread and commonly-observed minerals, and has the high fixation potential. The goethite frequently reveals acicular shape with finite dimensions along the a, b axes (<100nm) but infinitely long along the c axis. These small crystals cause shifts of XRD peak positions as well as broadening of the peaks. Therefore, the relation between the peak position and crystal size must be constructed. In this report, we calculated XRD patterns of goethite for eleven different lines with relative intensities over 10%, assuming that crystals are composed of the same number of unit cell piling up along both the a and b axes but infinite along the c axis.

Figure 1 shows calculated XRD patterns for 110 line of goethite with different crystal size, which is labeled as N (number of unit cell along both the a and b axes). As is shown in this figure, a smaller N value, i.e. a smaller crystal resulted in both broadening of peak and shift of the peak position, to larger degree for this line. As an indicator of the broadening, full width of a half maximum intensity (FWHM) was determined from the difference between two points at a half of maximum intensity, and peak position from average of the two. Figure 2 and 3 show their variations associated with an increase in the N values. The broadening following reducing the crystal size was commonly observed in any other line, while direction of peak shift was diverse. A curve in the figure 3 is derived from the Scherrer equation (Scherrer constant=1.5), which is used to approximately determine the crystal size from the XRD peak broadening. The calculated data in this study were well corresponded to the Scherrer curve and the propriety of this calculation was verified. The lattice parameter were calculated from

these peak positions at different crystal sizes. Deviations due to differences in the crystal sizes were found to have the same magnitude as those due to aluminium substitution for iron in the goethite crystals. This means that correction is indispensable for an accurate XRD peak position for a small crystal.

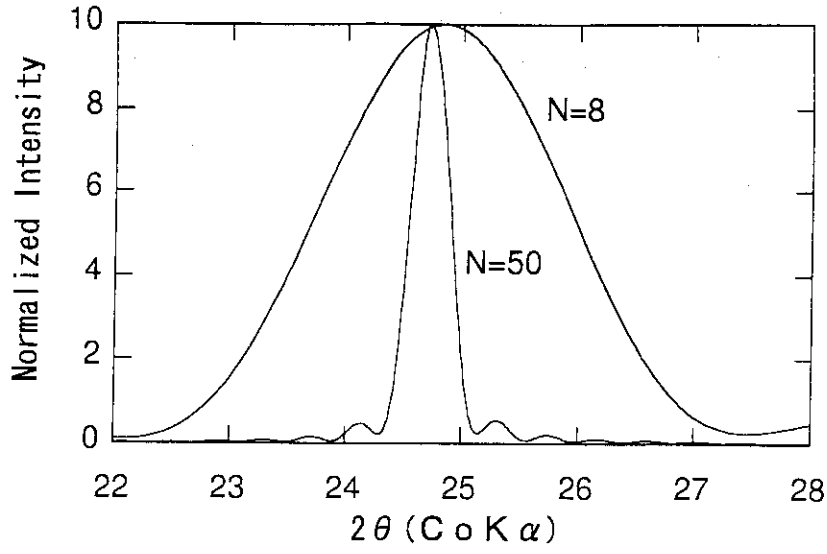

Figure 1 Calculated XRD patterns for goethite 110 line with 8 x 8 and 50 x 50 unit cells along a and b axes.

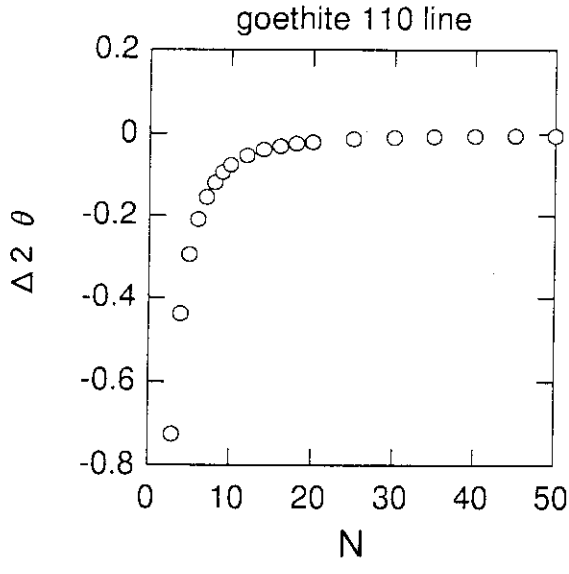

Figure 2 Peak shifts v.s.the number of unit cells.

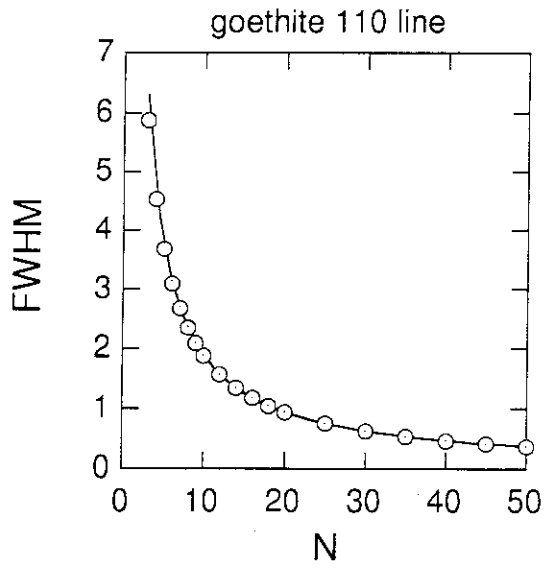

Figure 3 FWHM v.s. the number of unit cells and the Scherrer equation.

3.2 Nuclide Migration

3.2.1 Radionuclide Migration Experiments under In-situ Conditions*

T.T. Vandergraaf, D.J. Drew; AECL Research Whiteshell Laboratories, Pinawa Manitoba, Canada ROE 1L0
M. Kumata; Japan Atomic Energy Research Institute, Tokai Ibaraki 319-11 Japan

In virtually all concepts for the disposal of high level wastes, one of the roles of the geosphere is to serve as a natural barrier to radionuclide migration by impeding or retarding the movement of any radionuclides released from the waste to the biosphere. Retardation of radionuclide transport results from the interaction of dissolved radionuclides with the minerals present in fractures that form flow paths for the groundwater and with the surfaces of the interconnected pore space in the rock matrix surrounding a disposal vault. This interaction is usually represented numerically by a sorption coefficient that expresses sorption as a ratio between the concentrations of a radionuclide sorbed on a surface to that remaining in solution.

The interactions between radionuclides and geological surfaces are complex and are controlled by a large number of parameters including the chemical behaviour of the radionuclide, the chemical and mineralogical properties of the geological surface and the chemical composition of the groundwater, including the concentration of major and minor species, pH, Eh, and competing species.

In designing experiments to study the migration of radionuclides under the conditions expected in the rock mass surrounding a disposal vault, care needs to be taken to ensure that similar conditions are imposed. Over the past five years, we have performed a series of migration experiments in a specially designed facility at the 240 Level of AECL's Underground Research Laboratory (URL) near Lac du Bonnet, Manitoba (Figure 1).[1,2] These experiments were performed in columns of crushed material taken from a major fracture zone in the URL and using mildly reducing groundwater obtained directly from this fracture zone. By pumping this groundwater directly from the fracture zone into the crushed rock columns, exposure to atmospheric oxygen was avoided and in situ conditions maintained. The results from these experiments showed that multivalent radionuclides such as Tc, were strongly retained on the column material. even after 3000 hours (Figure 2). presumably by reduction of TcO_4^- to Tc(IV) by Fe(II)-containing minerals such as biotite or magnetite. The observed retardation was much higher than that predicted from sorption coefficients obtained on identical geological material in static sorption experiments in a glove box under an atmosphere containing <0.5 ppm oxygen, suggesting that these low concentrations of oxygen in chambers with controlled atmospheres

are still sufficiently high to prevent the reduction of TcO_4^- to TcO_2 by ferrous iron in the static sorption experiments.[1] Similar results were obtained for the multivalent actinides Np and Pu.[2]

To augment these 1-D migration experiments in columns of crushed fracture infilling materials with experiments in natural fractures under in situ conditions, a new facility, the Quarried Block Radionuclide Migration Facility (QBRMF), has been designed and is currently being constructed at the 240 level of the URL (Figure 3), adjacent to a natural, vertical, water-bearing fracture, JZ2. The design of this new facility is based on that of an existing laboratory at the Whiteshell Laboratories. the Large Block Radionuclide Migration Facility.[3] The QBRMF has been designed to be licensed as a Class B Radioisotope Laboratory, allowing the use of small quantities of actinides and fission products. Blocks of granite with dimensions of 1 x 1 x 0.7 m and containing part of JZ2 will be excavated from the wall of the QBRMF adjacent to JZ2 using a diamond wire saw and used in migration experiments with groundwater pumped directly from JZ2 into the blocks. This Facility will allow migration experiments to be performed under in situ conditions and also allow the radiometric analysis of the flow field at the completion of the migration experiments .[4,5]

References

1. Kumata, M. and T.T. Vandergraaf. 1993. Technetium behaviour under deep geological conditions. Radioactive Waste Management and the Nuclear Fuel Cycle 17(2), pp. 107-1 17.

2. Kumata, M. and T.T. Vandergraaf. 1992. Migration behaviour of long-lived radionuclides under deep geological conditions. 29th International Geological Congress, Kyoto, Japan, 1992 August 24-September 3 .

3. Drew, D.J., D.M. Grondin and T.T. Vandergraaf. 1990. The Large Block Radionuclide Migration Facility. Atomic Energy of Canada Limited Technical Record TR-519.

4. Vandergraaf, T.T and D.J Drew. 1991. Laboratory studies of radionuclide transport in fractured crystalline rock. ~n Proceedings of the Third International Symposium on Advanced Nuclear Energy Research - Global Environment and Nuclear Energy. Mito City, Japan, 1991 March 13-15. pp. 385-393.

5. Vandergraaf, T.T., D.J. Drew and S. Masuda. 1994. Radionuclide migration experiments in a natural fracture in quarried blocks of granite. Accepted for publication in a special issue of Radiochimica Acta devoted to Migration '93 .

---

* This study was presented at the 6th Annual International Conference on High-Level Radioactive Waste Management, Las Vegas, USA, April 30- May 5, 1995.

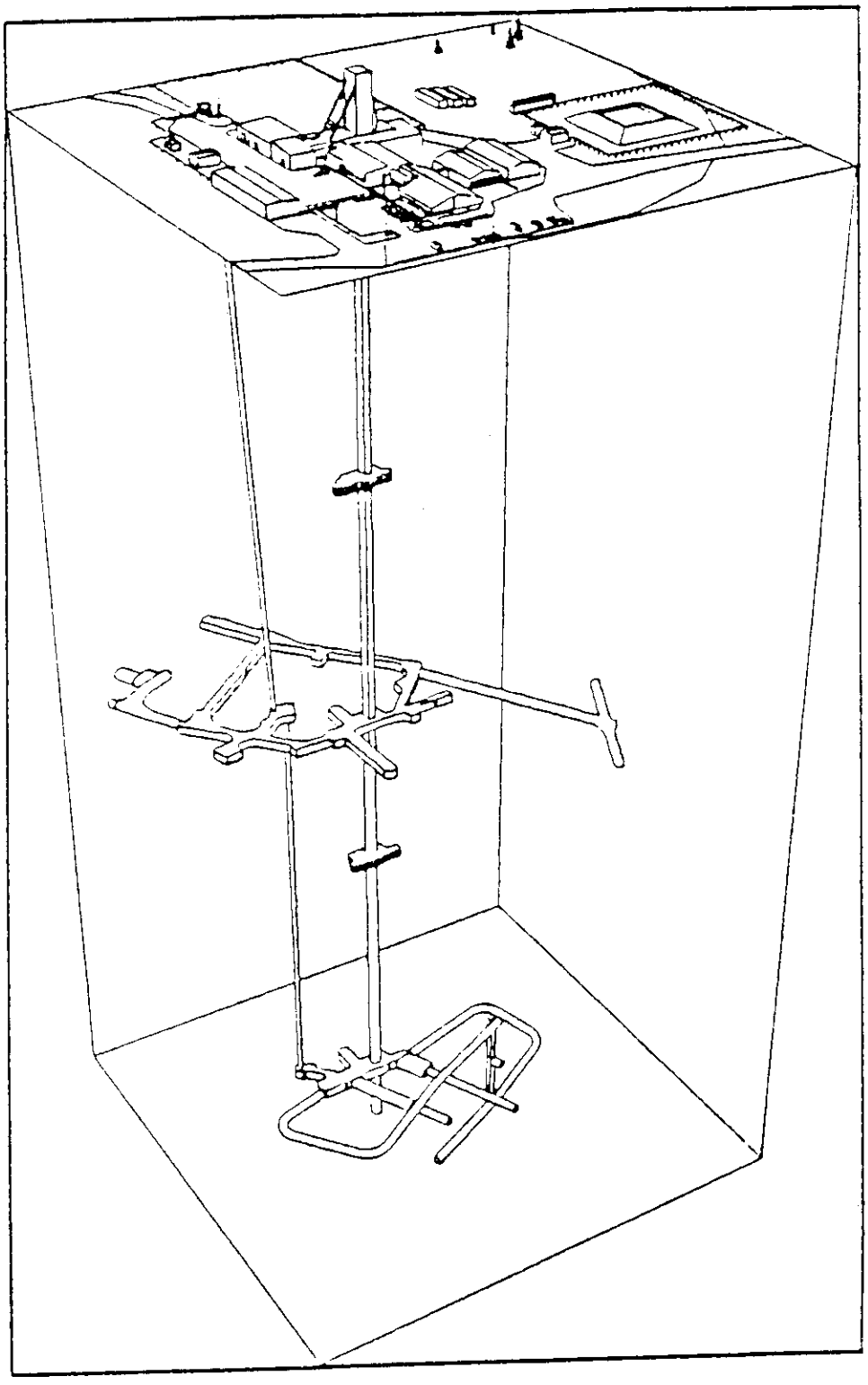

Figure 1: Isometric view of the Underground Research Laboratory near Lac du Bonnet, MB

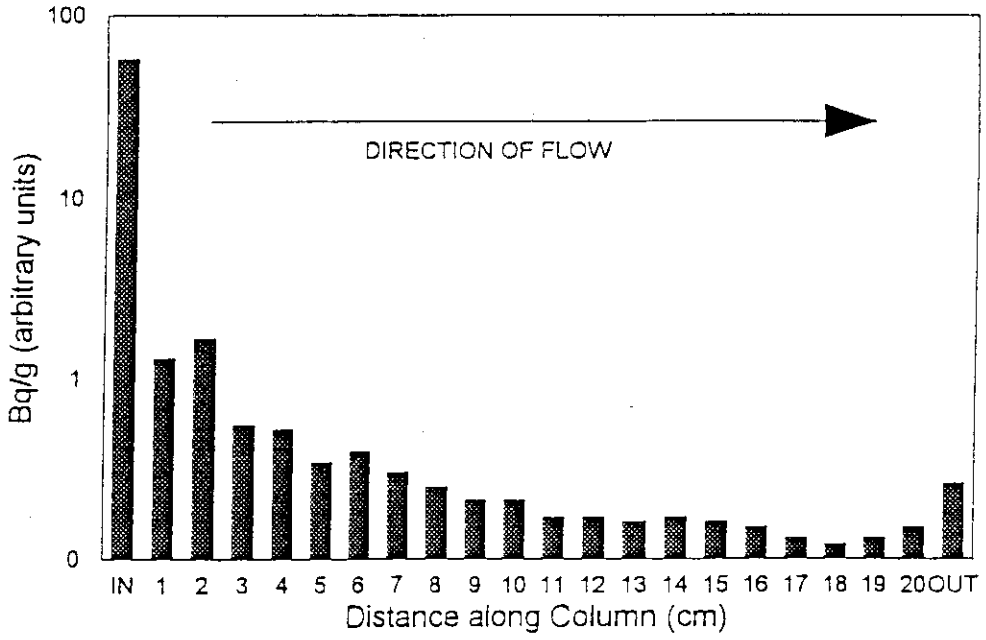

Figure 2: Activity Profile of ^{95m}Tc along column of crushed granite used in migration experiments after 2000 h @ flowrate of 2 mL/h

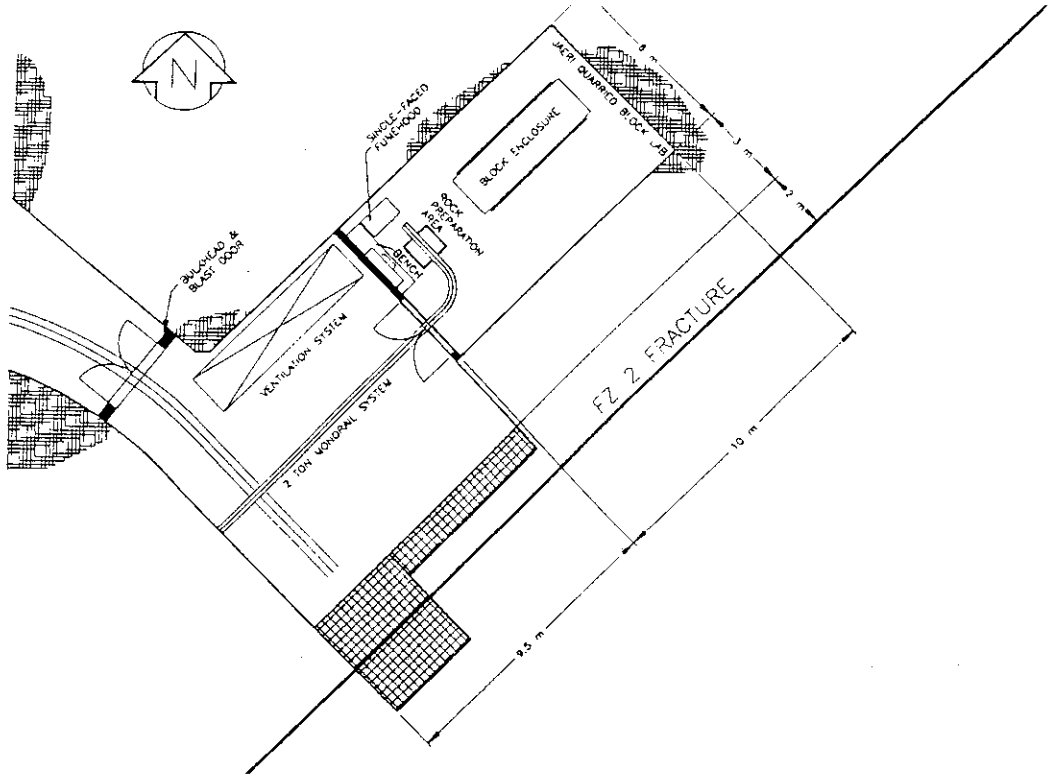

Figure 3: Layout of the Quarried Block Radionuclide Migration facility at the 240 level of the Underground Research Laboratory. Cross matched area to be removed by mechanical excavation to prevent damage to the fracture

3.3 Natural Groundwater Flow System

3.3.1 Physical Model Simulation Tests for Resistivity Tomography[1)]

Masahiro KUMATA*, Hiroyuki Ii** and Akihiko Chiba***
*Japan Atomic Energy Research Institute, Tokai-mura, Ibaraki, 319-11 Japan
**Japan Atomic Energy Research Institute (present address, Sumiko Consultant Co., Ltd., Shinnjuku, Tokyo, 160 Japan)
***Sumitomo Metal Mining Co., Ltd., Shinnjuku, Tokyo, 160 Japan

Abstract

Physical model simulation tests were performed using a tank 2 x 2 m square and 2.2 m deep filled with an NaCl solution and four mechanically moving electrodes. Two different configurations of double fracture model using copper prisms were set in the tank respectively. One was a parallel fracture configuration (Case 1) and the other a skew fracture configuration (Case 2). The electric potential field in an area selected for the experiment was measured by pole-pole array. Comparing the reconstructed images obtained by inverting data of Cases 1 and 2 indicates the effects of the three-dimensional structure on the cross section of the tomography. Numerical simulations corresponding to the tank experiment were performed for the parallel configuration of the double fracture model. The reconstructed images suggested that the apparent resistivity of the copper prism may be higher than its actual resistivity in the tank.

Introduction

In the case of resistivity tomography, geological cross sections are visualized by reconstruction of the data obtained from measurements of the electrical potential in the ground. To fully understand the reconstructed cross section from the resistivity tomography, the detection limit and/or resolution of the technique should be discussed. Although numerical model calculations can handle the problem with digital computers, the verification of these results is difficult without supporting experimental work. For this purpose, an experimental approach was planned using a physical model simulation technique based on a tank filled with an NaCl solution (Kumata et al., 1993). By using this technique, the effects of the three-dimensional distribution of electrical potential in cross section (two-dimensional view) of the resistivity tomography can be studied.

For comparison with the results of the physical model simulation, numerical experiments were carried out by using the 2.5 dimensional finite element method (FEM). The electric potential field was calculated by applying the theory of images. In resistivity inversion,

the DLST method was used. Boundary conditions of the model were based on the real tank. The model was composed of a background resistivity of 20 Ω m and two fractures of 10^{-6} Ω m.

Experimental apparatus

The experimental apparatus consists of a steel tank and three sub-systems (Fig.1). The tank, 2 x 2 m square and 2.2 m deep, was filled with an NaCl solution of resistivity 20 Ω m to a depth of 2 m. All surfaces of the tank walls were coated with a special insulating paint to electrically isolate the inside of the tank (Goudswaard, 1957). An ohmmeter showed more than 500 k Ω between the inside and outside walls of the tank at all points.

The cross section to be used in the experiments was set along the center line of the tank. Four electrodes were set in a 50 cm x 50 cm square within the cross section using mechanical actuators. Each electrode was computer controlled to move to any position in the area with a location accuracy of 0.1 mm.

A square wave current of 12 seconds duration and 50 % duty cycle was transmitted at from 6 to 96 V into the liquid from the current source electrode, and potentials were measured in the measurement system. Measured potentials and applied currents were converted to digitized time series data by a 12 bit A/D converter and then recorded to floppy diskette. Both potential and current were amplified and conditioned by a 20 Hz low pass filter. The electrode actuation and measurement systems were maintained by the control system with a personal computer.

Fracture model

Since fractures with clay minerals and/or groundwaters are generally detected as low resistivity anomalies, pure copper (resistivity of about 10-6 Ω m) was selected as a fracture model material. Two 1.2 m long copper prisms of square cross sections with 4 cm sides were prepared to represent conductive fractures.

Physical model simulation

Experimental cross section

Initially, for the selection of the most effective area for the physical model simulation, the electric field in the whole tank was observed using pole-pole, pole-dipole and dipole-dipole arrays with a multi-electrode and measuring equipment, including a scanner and a transmitter. The multi-electrode contained twenty-seven pieces of 2 or 3 mm wide copper tape as potential electrodes and was suspended with a weight in the NaCl solution. The top electrode was placed

just on the solution surface and the lowest electrode was 180 cm beneath the liquid surface. Electrode spacing varied from 2 cm to 20 cm depending on the location of the electrode. The multi-electrode was moved and stopped 50 times along the center line of the tank to observe the electric field in the whole tank. Data were obtained a total of 1310 points on the cross section along the center line. During the observation, the current electrode was positioned in the center of the surface line. In the case of the pole-pole and pole-dipole arrays, an infinite electrode for current was positioned close to the wall in the tank. The position of (X,Z)=(0,0) was set at the center of the water surface in the tank.

Further, the electric field in the area of 50 cm x 50 cm ($-25 \leqq x \leqq 25$ cm, $0 \leqq z \leqq 50$ cm), a part of the cross section, was observed in detail using four electrodes with mechanical actuators. The length of the potential dipole was set at 2 cm for the pole-dipole array. In the case of the dipole-dipole array, the dipole length was fixed at 4 cm.

Equipotential contour maps in the 50 cm x 50 cm area and in the whole tank filled with an NaCl solution were obtained by using three arrays respectively. On the basis of these contour maps, a square area 20 cm x 20 cm ($-10 \leqq x \leqq 10$ cm, $0 \leqq z \leqq 20$ cm) to be used in the experiments was selected.

Fracture model experiment

Double fracture model; To examine the effects of three dimensional structure on the tomography, two copper prisms of square cross section with 4 cm sides were used in two different configurations (Fig.2). One is a parallel fracture configuration (Case 1) and the other is a skew fracture configuration (Case 2). Electrodes were set around the selected area except the lower side in the experimental section (Fig.3). The cross sectional area of the copper prism cutting the experimental section were almost the same in both Cases 1 and 2. The electric field in the experimental section was observed using a pole-pole array.

Before the start of physical simulation tests with fracture models, blank tests were carried out.

Effects of three dimensional structure

Reconstructed images of the tank experiment double fracture model obtained by inverting pole-pole data are shown in Figure 4. Comparing Cases 1 and 2 indicates that although both reconstructed images do not indicate two separate fractures, the shapes of the images are obviously different. The reconstructed image of the skew configuration is elongated in shape whereas that of the parallel configuration is more rounded and could be interpreted as a single fracture. The reconstructed image of the skew configuration appears to define the lower fracture.

Measured apparent resistivity distribution maps are also shown in Figure 4. The numbers on the ordinate and abscissa of the map indicate the positions of potential and current electrodes respectively. The apparent resistivities were plotted on the map at the corresponding electrode number. The apparent resistivity distribution maps are useful to check the data. When good data are measured, the distribution map is symmetric with respect to the center point. Maps showing disturbed symmetry indicate poor data. The maps for the tank experiments in Figure 4 show almost symmetrical distribution. Accordingly, the difference of reconstructed images of Cases 1 and 2 is considered as the effect of three dimensional structure on the tomography.

Numerical simulation

Numerical simulations corresponding to the tank experiment were performed for the parallel configuration of the double fracture model and results are shown in Figure 5. Conditions of Model-1 and Model-2 in Figure 5 are the same except for the resistivity of the fracture (copper prism). The reconstructed image of Model-1 was obtained by inverting pole-pole data with a fracture resistivity of 10-6 Ω m. Model-2 was calculated with 0.6 Ω m fracture resistivity. Neither image is the same as the results obtained from the tank experiments, however, it seems that numerical simulation result for Model-2 is rather similar to the tank result. This might mean that the resistivity of the copper prism is apparently changed to approximately 0.6 Ω m in the tank. It may be considered that the effect of electrochemical reactions on the surfaces of the copper prism in the electrolyte solution appeared.

Conclusion

The experimental system using a tank filled with an NaCl solution worked well for physical model simulation of resistivity tomography. The reconstructed images showed the effects of the three-dimensional structure on the cross section of the tomography.

The reconstructed images obtained from numerical simulations suggested that the apparent resistivity of the copper prism may be larger than actual resistivity in the tank.

References

Kumata, M., Chiba, A. and Kubota, R., 1993, Model tank experiments for basic study on resistivity tomography: 1993 SEG 63rd Annual Meeting, September 26-30, Washington, D.C., U.S.A.

Goudswaad, W., 1957, On the effect of the tank wall material in geoelectrical model experiments: Geophysical Prospecting, 5, 272-281.

---

1) This study was presented at the 3rd SEGJ/SEG International Symposium on the Geotomography - Fracture Imaging -, Tokyo, Japan, November 8-10, 1995.

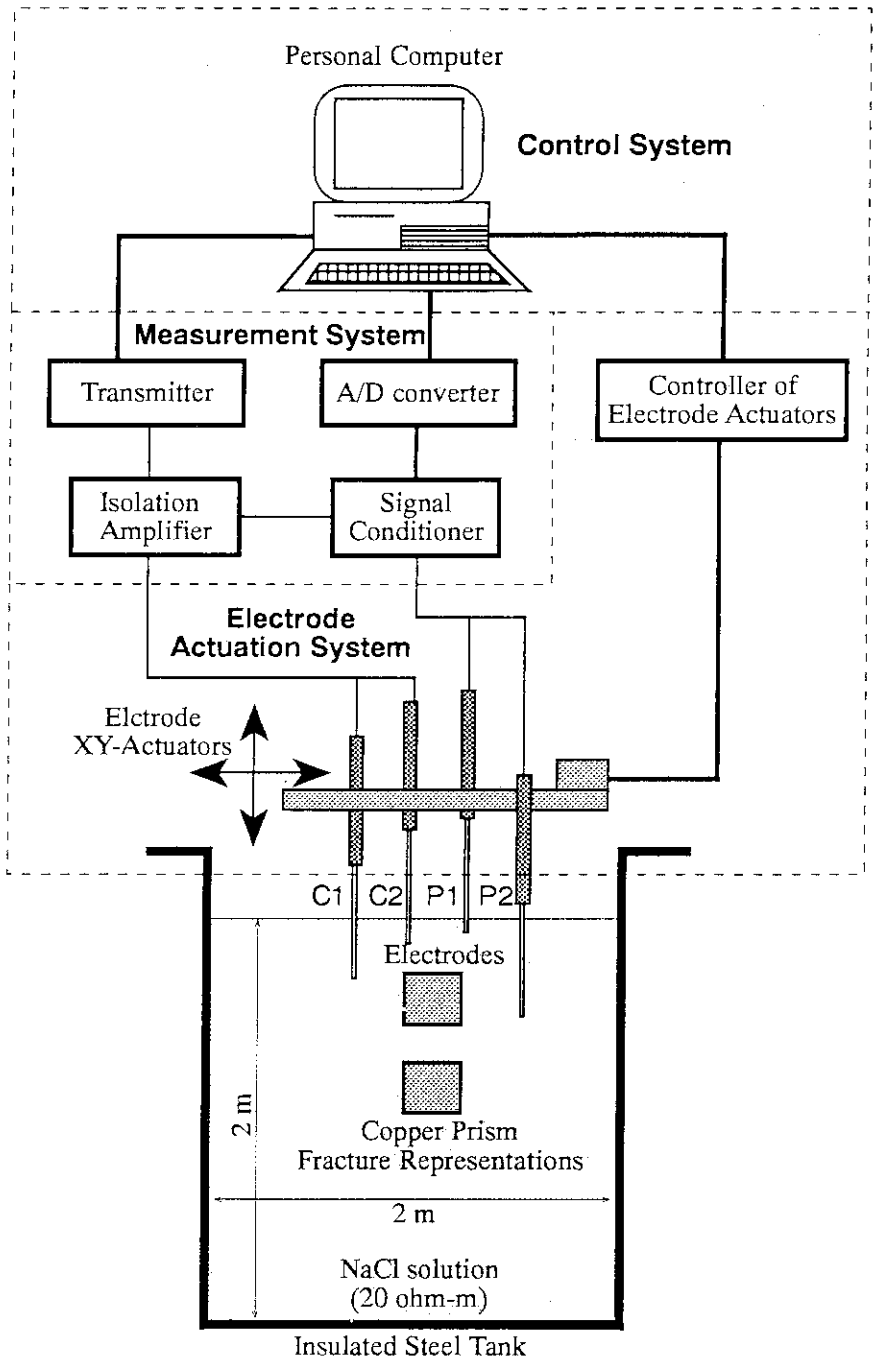

Fig.1 System Diagram of Tank Experiment for Resistivity Tomography

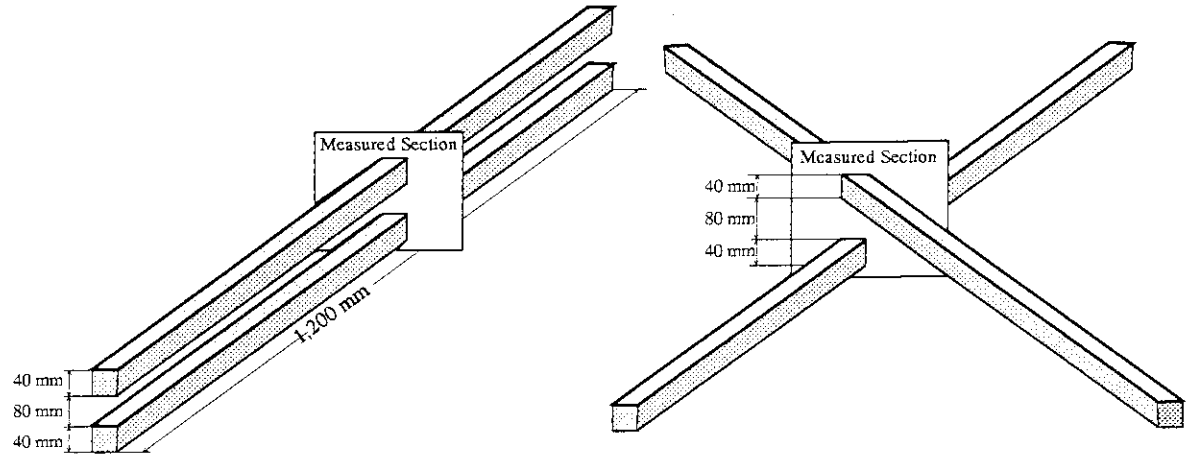

Case-1: Parallel Fracture Configuration　　Case-2: Skew Fracture Configuration

Fig.2 Experimental configurations of two copper prism fracture representations

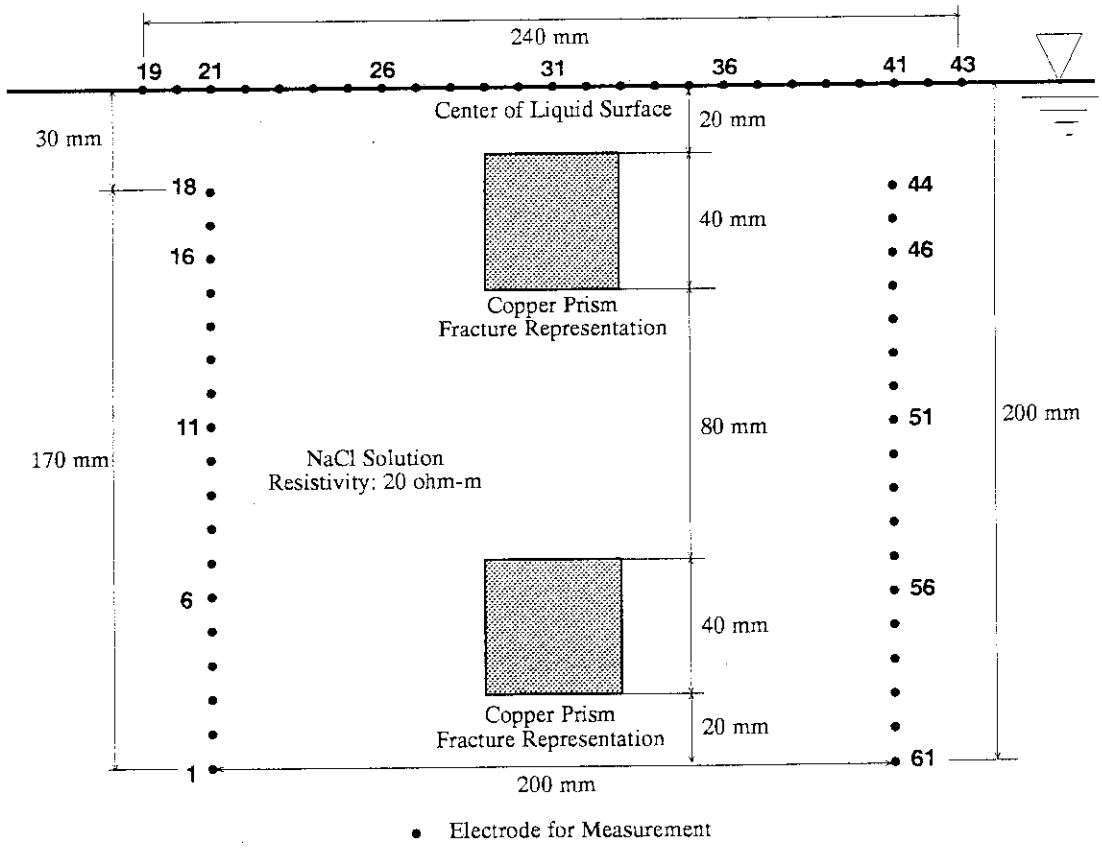

Fig.3 Location of 61 Electrodes and Two Copper Prism Fracture Representations

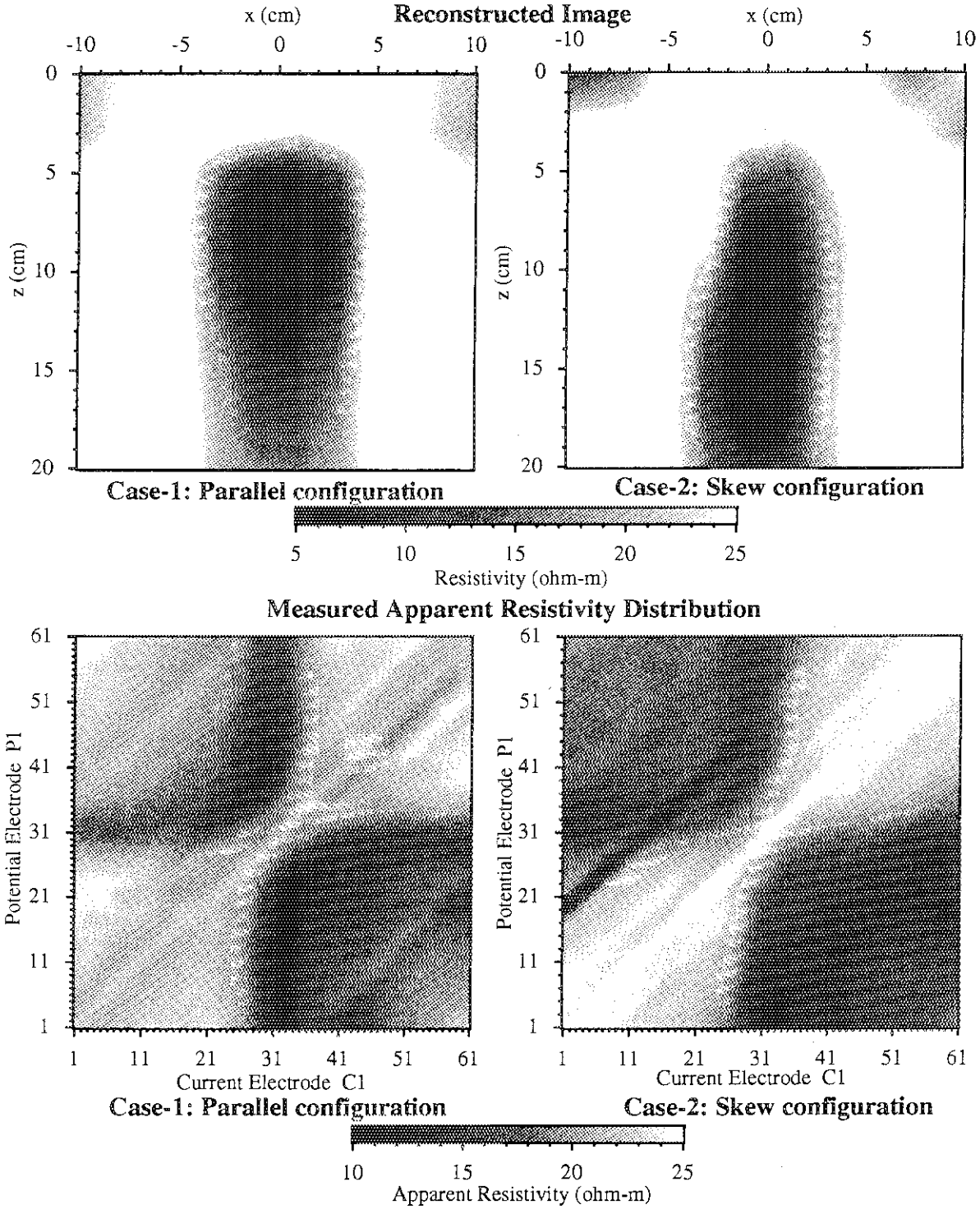

Fig 4 Results of Tank Experiment for the Double Farcture Model
Reconstructed images and measured apparent resistivity distribution maps were obtained by pole-pole array.
Case-1: Parallel configuration of 2 copper prism fracture representations.
Case-2: Skew configuration of 2 copper prism farcture representaions.
Resistivity of NaCl solution filled with tank: 20 ohm-m

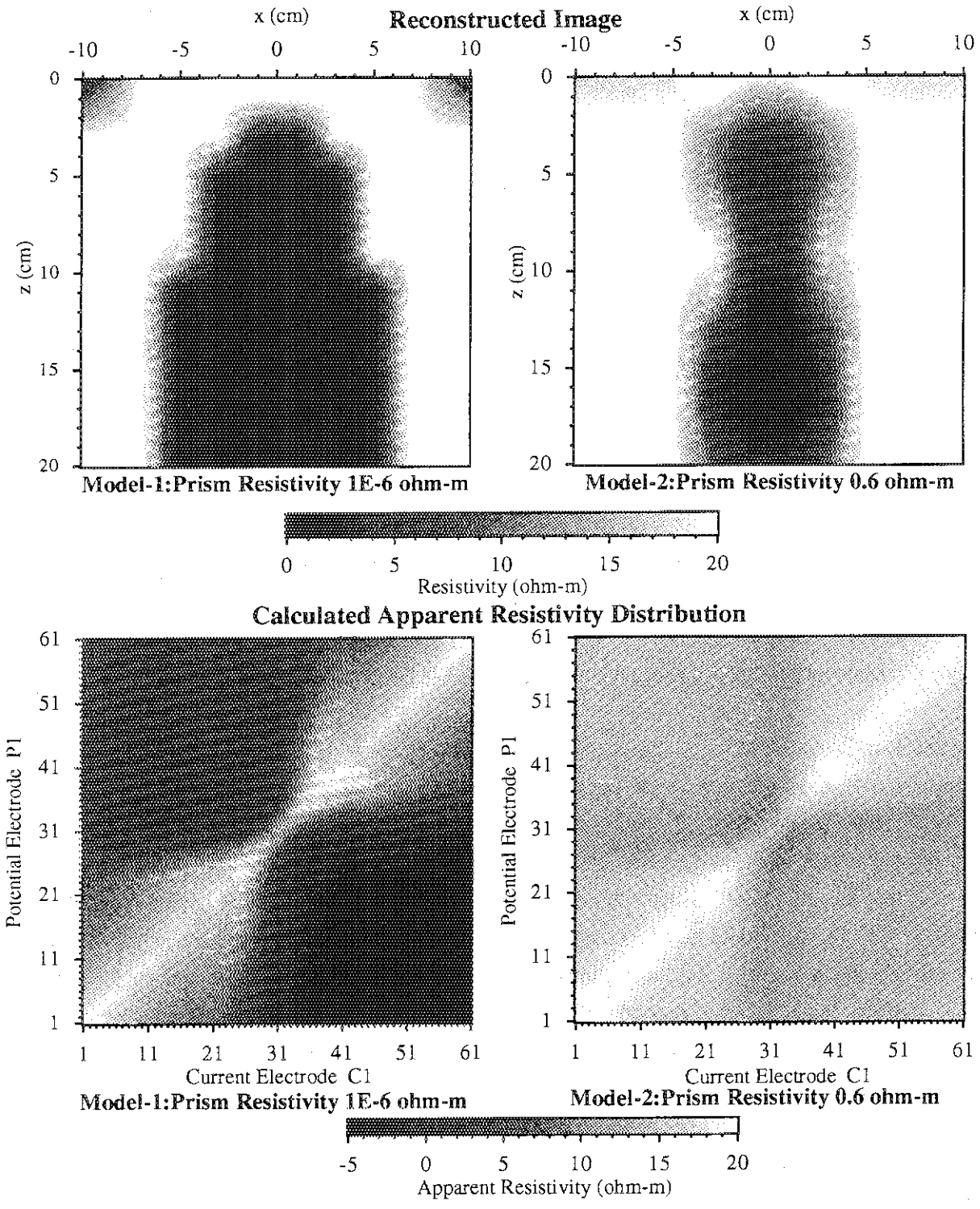

Fig 5 Results of Numerical Simulation for the Double Fracture Model
Two model resistivities on same parallel fracture configuration are shown as reconstructed images and apparent resistivity distribution maps by pole-pole array.
Bouckground Resistivity: 20 ohm-m

3.3.2 Comparison of pole-pole array with pole-dipole

H. Iwamoto and M. Kumata

INTRODUCTION

In the resistivity tomography, the potential difference between two electrodes is measured during the electrical current is flowed between another two electrodes. There are three measurement methods in the resistivity tomography, because of the difference of electrode's array. These are called pole-pole array, pole-dipole array and dipole-dipole array.

The purpose of this study is to know the differences of the resolution of the pole-pole array and pole-dipole array, using the tank experiment which simulates the rock mass and fractures.

TANK EXPERIMENT

A steel tank 2*2 m square and 2.2 m high was prepared. All surface of the tank walls were coated with a special insulating paint.

The tank was filled to depth of 2 m with a NaCl solution of resistivity 20 ohm-m.

Two copper's rectangular solid as the sham fractures were arranged in the tank (show Figure-1). The resistivity of copper is about 10^-6 ohm-m.

The method of measurement for resistivity tomography were pole-pole array and pole-dipole array. The number of electrode sets were above 3,000 at the both case.

INVERSION ANALYSIS

As first step, the "measured apparent resistivities" were obtained for all electrode set with the measured data.

As second step, the cross section divided into 123 blocks for resistivity (show Figure-2). The positions of two sham fractures in the tank experiment were equal to No.18,19,30,31,90,91,102 and 103 on Figure 2. Then the potential distribution was calculated for the cross section with 2.5D finite element method (FEM) on the assumption that 123 blocks are 20 ohm-m. Based on this potential distribution, the initial "calculated apparent resistivities" were obtained for the same electrode set corresponding to the tank experiment.

As next step, the resistivities of 123 blocks were modified with the nonlinear least-squares method in order to obtain the new "calculated apparent resistivities" that is closer to the "measured apparent resistivities" than initial one. The potential distribution was recalculated with the modified resistivities of 123 blocks and FEM. And the second "calculated apparent resistivities" were obtained based on the modified data.

The above calculation was iterated until a mean-squares error introduced from two apparent resistivities group became a minimum. If the error had been decreasing ,the calculation was stopped when the iteration number reached a limited number.

Finally, the resistivity of 123 blocks when the iteration stopped was an output to make a reconstructed image.

RESULTS AND DISCUSSION

Figure-3a (pole-pole array) and Figure-3b (pole-dipole array) are reconstructed images, and these are drawn as the contour map obtained from the output of inversion analysis.

In the case of pole-pole array, there aren't two parts of the low-resistivity but only one part in Figure-3a. And moreover, the size of this is bigger than the actual one, and the position is deeper than the actual one. In the case of pole-dipole array, there are two low-resistivity parts in Figure-3b. An upper part of the low-resistibity was is the actual size and the depth, but an lower part is different from the actual one.

These results show that the pole-dipole array is better than the pole-pole array as regards the resolution, because there is no difference on the treatment of calculation for two method. However, the result of pole-dipole array doesn't show a satisfying reconstructed image in the existing circumstances.

FUTURE WORKS

In the theory, if the analysis program what simulates the tank experiment is used instead of the tank examination, the result of the inversion analysis is equal to the input data into this tank simulation program. However, it is not so actually. There are some subjects to make clear this phenomenon. It is one of the most important subject what are the most suitable of the artificial noises added into the nonlinear least-squares method. And it is another subject whether 123 resistivity blocks are the suitable for this model, e.g. the number of the blocks and the size of a block.

After the above subjects are studied in detail, it is need that the features of the reconstructed images giving by the differences of the electrode's array give are compared again.

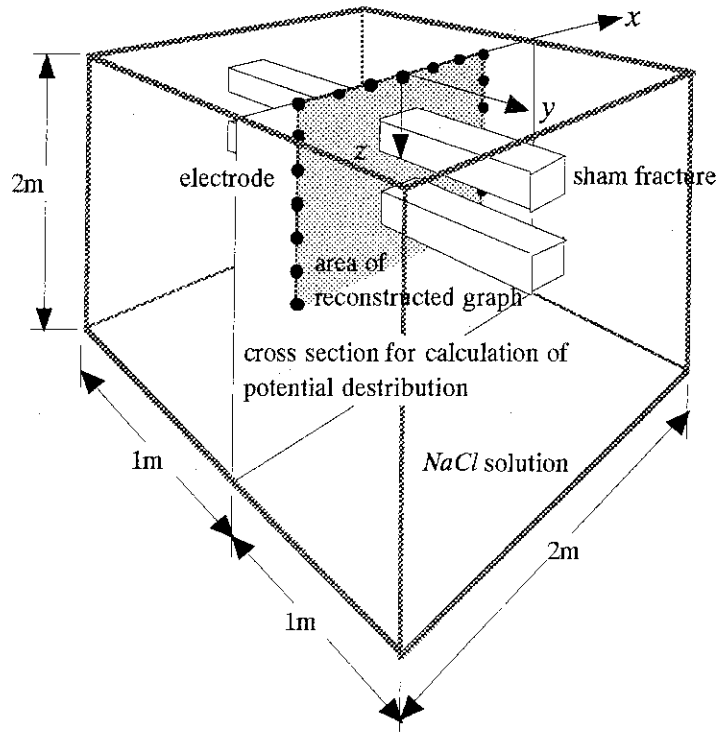

(a) a bird's eye view

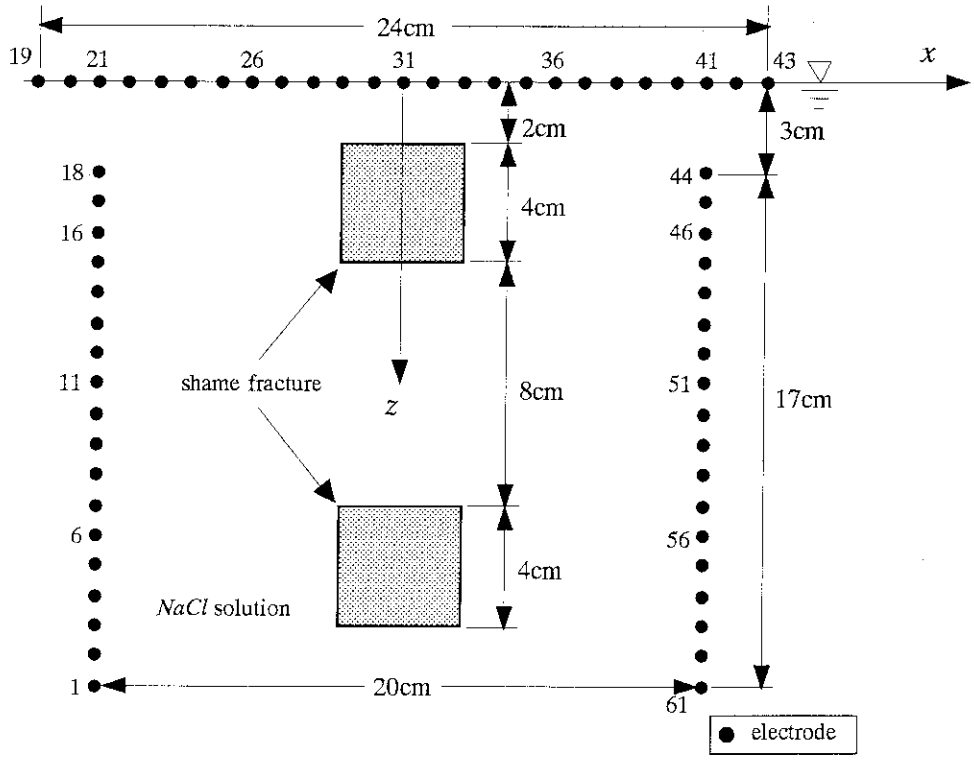

(b) pattarn of electrodes

Figure-1 the relationship between the elctrode and the sham fractures

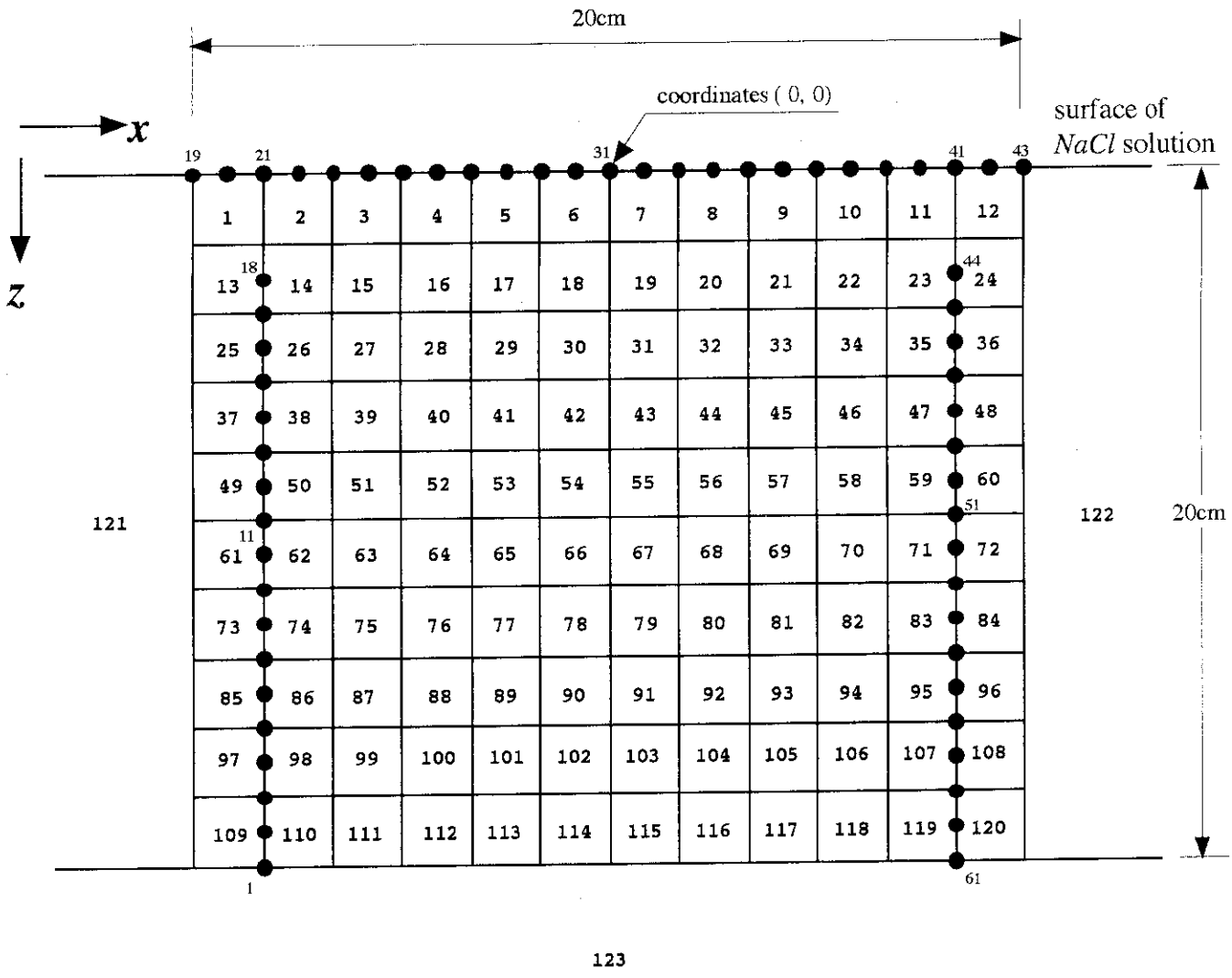

17 resistivity block for inversion analysis

61 electrode

Figure-2 resistivity blocks

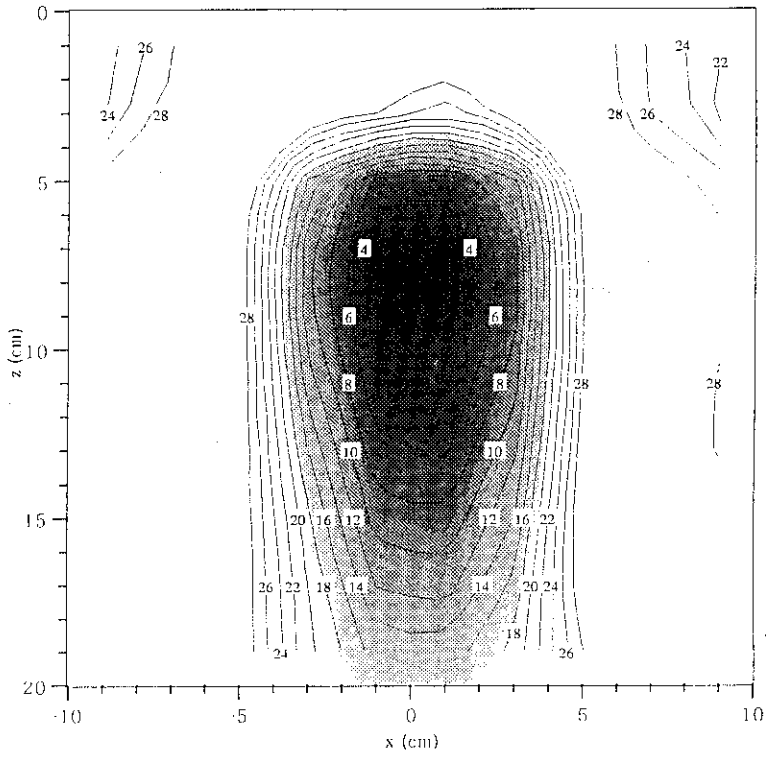

(a) pole-pole array

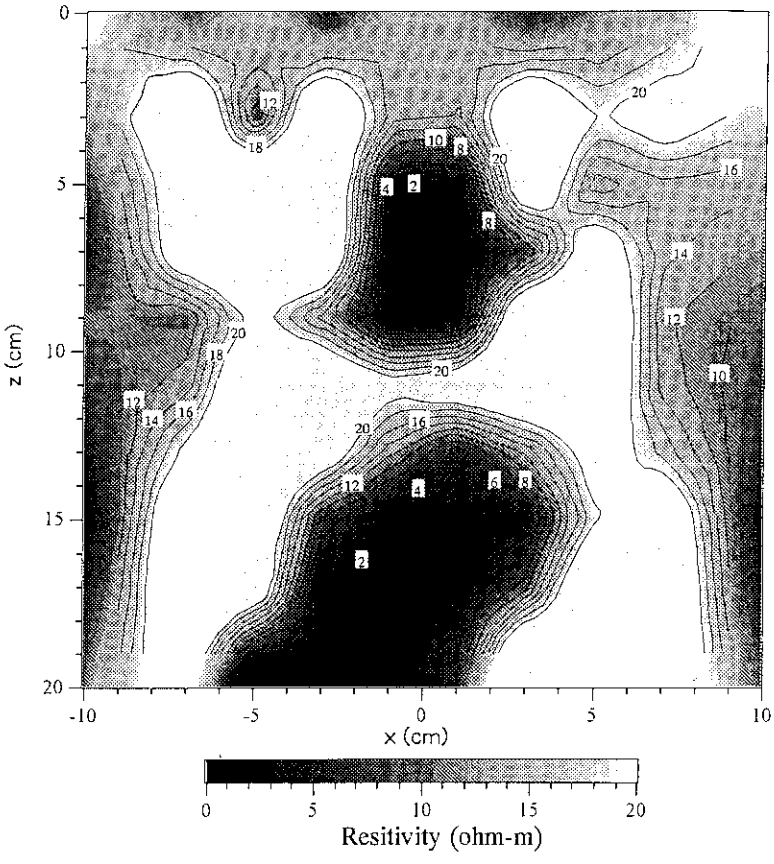

(b) pole-dipole array

Figure-3 reconstructed image

3.4 Natural Analog

3.4.1 Natural Analog Study

T. OHNUKI, N. YANASE, H. ISOBE, T. SATO,
T. NAGANO, Y. IIDA, K. SEKINE

The objectives of the natural analog studies are to evaluate the concept and/or mathematical models and parameters for assessing the impact of geological disposal of radioactive wastes. The information obtained in the natural analog studies can make significant contribution on a support to the construction of the performance assessment scenario, and on a presentation of the direct evidence of long term retention of elements in geological condition. JAERI has been carrying out the natural analog studies at three uranium ore deposits; Koongarra (Australia), Oklo (Gabon) and a sandstone type deposit in Japan.

a) Koongarra, Australia

JAERI has participated in the OECD/NEA analog project, Analog Studies in the Alligator Rives Region (ASARR) and has been working on the migration behavior of uranium series nuclides through a rock system during the weathering process from chlorite to kaolinite.

The rock samples were collected from DDH-4 drill core several ten meters downstream of the secondary ore deposit. To clarify centimeter order behavior of uranium the powdered samples were contacted with several different reagent solution to dissolve uranium from different minerals of the rock sample (selective extraction tests). To clarify interaction between uranium and minerals, the thin sections of the rock samples were observed by high resolution transmission electron microscopy (HRTEM) and analytical electron microscopy (AEM).

In the selective extraction tests the highest amount of uranium was dissolved by the CDB reagent solution which dissolve crystalline iron minerals (Fig. 1). This shows that uranium is preferably accommodated with crystalline iron minerals. A hot 6 M HCl solutions which dissolve clay mineral components of calcium and/or magnesium dissolve little uranium. Thus, uranium is not fixed to clay minerals.

By HRTEM observation uranium bearing phases 1-20 nm in size were surrounded by goethite, hematite and probably ferrihydrite. The uranium phases has preferred orintation to the iron minerals and phosphate and magnesium were detected by AEM. These suggest that uranium is crystallized to form saléeite, U-Mg phosphate mineral, at the surface of the iron minerals.

The uranium concentrations in groundwater downstream the secondary ore is approximately

several tens ppb. No uranium minerals should be precipitated from the groundwater by the calculation based on the thermodynamic data for uranium minerals. Saturation with respect to saéeite is not abtained from the groundwater with higher Mg^{2+} and HPO_4^{2-} concentrations by a factor of 100. The Koongarra groundwater is poorer in uranium and phosphate concentrations downstream the secondary ore deposit than saturation concentration of saléeite, but microcrystals of saléeite are formed by catalysis of iron minerals.

b) Oklo, Republic of Gabon

Oklo uranium ore is one of adequate natural analog sites for geological disposal, because it has preserved abundant fissiogenic nuclides for 2 Ga. JAERI has been studying the migration behaviors of TRU elements and FP based on the isotopic compositions and chemical compositions of minerals analyzed by JAERI and Hiroshima University under cooperation research program. The concentrations of FP nuclides at different reactor zones (RZ) show that rare earth elements and platinum group elements are retained in the RZs. While approximately 10 % of alkaline metal elements and alkaline earth elements were retained in the RZs.

c) A sandstone type deposit in Japan

The rock samples of granite below the ore collected in Japan were analyzed by neutron activation analysis to measure the concentration of rare earth elements (REE). In the granites of different weathering degrees the concentrations of light REE (La, Ce) have positive correlation to that of uranium. While no correlation was detected between the concentrations of heavy REE (Yb, Lu) and uranium. These suggest that elements of different properties have fractionated during weathering process of granite.

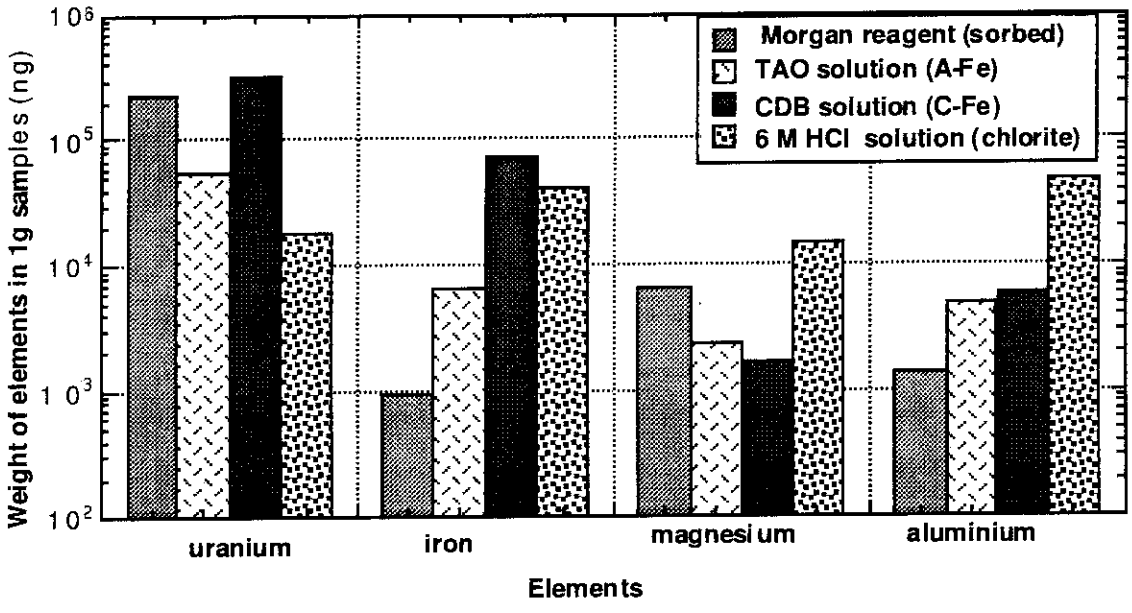

Fig. 1 Quantity of dissolved elements weight from the rock samples obtained from the DDH4 core hole at 21 m in depth with different reagent solutions. The relationships between the reagent solutions and the elements dissolved are as follows:
Morgan reagent: elements sorbed on minerals,
TAO solution: elements associated with amorphous iron minerals and manganese oxides,
CDB solution: elements associated with crystalline iron minerals, and
6 M HCl solution: elements retained by minerals other than quartz.